ISSN 2812-9474

Engineering TODAY

VOL. 1 / NO. 1 / 2022

PUBLISHED BY

The Faculty of Mechanical and Civil Engineering
in Kraljevo of the University of Kragujevac

ISSN 2812-9474

VOL. 1 / NO. 1 / 2022

Engineering TODAY

PUBLISHED BY

The Faculty of Mechanical and Civil Engineering
in Kraljevo of the University of Kragujevac

Engineering TODAY

PUBLISHER

The Faculty of Mechanical and Civil Engineering in Kraljevo
of the University of Kragujevac

ADDRESS

Faculty of Mechanical and Civil Engineering
Dositejeva 19, 36000 Kraljevo
Republic of Serbia

CONTACT

Tel: +381 36 383 269
+381 36 383 377
+381 36 383 378

Fax: +381 36 383 269

Email: editor@engineering-today.com

Web: www.engineering-today.com

FREQUENCY

4 issues per year

PRINTED BY

Grafika Galeb d.o.o, Niš

CIRCULATION

50 copies/issue

INSTRUCTION FOR AUTHORS

A Engineering TODAY manuscript should by written clearly and concisely in correct English. The length of a reviewing paper is up to 12 pages. All papers are subject to a reviewing process. Final acceptance of a paper for publication in the Journal is based on the decision of the Editorial Board.

TEMPLATE FOR MANUSCRIPT

Template can be downloaded from the journal's website.

SUBMISSION OF PAPERS

All manuscripts for consideration by the Engineering TODAY should be submitted via the journal's website.

CIP - Каталогизација у публикацији
Народна библиотека Србије, Београд

621(497.11)

ENGINEERING Today / editor in chief Radovan Bulatović. - Vol. 1, No. 1 (2022) - . - Kraljevo : The Faculty of Mechanical and Civil Engineering, University of Kragujevac, 2022 - (Niš : Grafika Galeb). - 30 cm

Tromesečno. - Je nastavak: IMK-14 = ISSN 0354-6829
ISSN 2812-9474 = Engineering Today (Kraljevo)
COBISS.SR-ID 64530953

AIMS AND SCOPE

Engineering Today is an international peer-reviewed scientific journal that publishes original papers, both theoretical and experimental, covering the whole spectrum of engineering sciences, but focusing mostly on mechanical, electrical and civil engineering. The primary objective is to provide a high-level platform for researchers and practitioners to disseminate theoretical or engineering-oriented research output achievements within the context of engineering systems that fosters knowledge sharing in different branches of engineering discipline.

Engineering Today also publishes novel theoretical methods, algorithms, simulations, experiments, and case studies as applications of state-of-the-art research in the field of engineering.

The topics of interest include, but are not limited to:

- Mechanical engineering
- Electrical/electronic engineering
- Civil engineering
- Manufacturing engineering
- Software engineering
- Thermal technique and environment protection
- Applied mathematics and physics
- Theoretical and applied mechanics
- Optimization algorithms
- Metaheuristic algorithms
- Railway engineering
- Earth-moving, construction and transportation machinery
- Automatic control and fluid technique
- Computer science
- Information systems
- Fault detection and diagnosis
- Learning systems
- Robust systems
- Neuro-fuzzy systems
- Internet of things
- Cybernetics
- System identification
- Stochastic systems
- Complex networks
- Computational complexity
- Mechatronics
- Production technologies
- Computer design and computer integrated processes design
- Design of machining processes
- Engineering management and entrepreneurship
- Mechanical construction and material technology
- Interdisciplinary applications

It provides an effective medium for researchers and a way to quickly publish high-quality original papers, so as to convey the latest important progress in their professional field to scientists in related disciplines. Engineering Today offers authors rigorous peer review, rapid publication, and maximum visibility. The journal expects to accept only the most relevant manuscripts and will provide very rapid evaluation to prevent publication delays. The Editors reserve the right to reject papers without sending them out for review.

From time to time, Engineering Today will publish review articles, short communications, discussions as well as special issues on a specific sub-field of engineering science. Authors are encouraged to contact the Editor-in-Chief if they would like to submit a review article or propose and edit a special issue of the journal.

Engineering
TODAY

VOL. 1 / NO. 1 / 2022

CONTENTS

ORIGINAL SCIENTIFIC PAPER OPEN ACCESS

Observer-Based Fault Estimation in Steer-by-Wire Vehicle

Vladimir Djordjević[1], Vladimir Stojanović[1*], Dragan Pršić[1], Ljubiša Dubonjić[1], Marcelo Menezes Morato[2]

[1] University of Kragujevac, Faculty of Mechanical and Civil Engineering in Kraljevo, Kraljevo, Serbia

[2] Universidade Federal de Santa Catarina, Departamento de Automação e Sistemas, Florianópolis, Brazil

ARTICLE INFO

[*] **Correspondence:** vladostojanovic@mts.rs

DOI: 10.5937/engtoday2201007D

UDC: 621(497.11) **ISSN:** 2812-9474

Article history: Received 17 January 2022; Accepted 8 February 2022

ABSTRACT

In this paper, the mechanism for the fault estimation (FE) problem for a steer-by-wire (SBW) vehicle with sensor and actuator faults is investigated. To deal with the design issues, we transformed the nonlinear model of SBW vehicle into a new coordinate system to jointly estimate the sensor and actuator faults. In the new coordinate system, the Lipschitz conditions and system uncertainties are also considered. The proposed schemes essentially transform the original system into two subsystems, where subsystem-1 includes the effects of actuator faults but is free from sensor faults and subsystem-2 only has sensor faults. Then two sliding mode observers (SMOs) are designed to estimate actuator and sensor faults, respectively. The sufficient conditions for the existence of the proposed observers with H∞ performance are derived and expressed as an LMI optimization problem such that the upper bounds of the state and fault estimation errors can be minimized. Finally, the numerical example with simulation results is provided to validate the practicability and efficacy of the developed estimation strategy.

KEYWORDS

Joint fault estimation, Sensor faults, Actuator faults, Steer-by-wire vehicle, Sliding-mode observer

1. INTRODUCTION

Modern control systems are prone to faults, which can damage the systems themselves or the environments in which they operate. For this reason, fault detection and isolation (FDI) algorithms become essential, since they enable fault-tolerant actions that minimize the effect of faults and improve the overall system's reliability and safety. The research on FDI has received considerable attention during the last two decades due to the increasing demand for safety and reliability of automatic control systems [1-2]. Naturally, the nonlinear control problem for different dynamics systems is always a hot topic and has attracted compelling attention from scholars, see [3-5].

The approaches of FDI developed in the past can be grouped into three fundamental categories: knowledge-based FDI methods, signal-based FDI and model-based FDI [6]. Among the possible approaches, the model-based FDI ones have been recognized as a handy tool by the scientific community and have been applied successfully to many physical systems, for example, lateral dynamics of a vehicle [7], aircraft [8], satellites [9], unmanned aerial vehicles (UAVs)[10], and wind turbines [11], among others. The basic idea of the observer-based FDI approaches, which fall into the category of model-based FDI, is to generally compare the actual system's behavior with the predicted or estimated behavior based on its mathematical model. Hence, the success of this type of technique directly relates to the mathematical model, which in reality is not a perfect representation. As a consequence, any discrepancies between the system and the model, which appear in the form of system uncertainties in the model, can cause a misleading alarm and make the FDI ineffective. Therefore, there is a need for a robust FDI which is sensitive to faults but insensitive to model uncertainties [12].

On the other side, fault estimation (FE) is different from the majority of fault detection and isolation (FDI) in the sense that it not only detects and isolates the fault, but also provides details of the fault, such as the location, size, and duration. Thus, it is especially useful for incipient faults and slow drifts, which are very difficult to detect. Also FE is vital in fault-tolerant control (FTC) systems which improve the system's performance. During the last two decades, considerable research results have been reported on FE. In [13], an online estimation approach based on adaptive observer technique was adopted to reconstruct the faults with an incipient time profile. A descriptor system approach was introduced to investigate sensor fault diagnosis for nonlinear systems in [14], which is applicable for sensor faults of any forms. Most physical systems are nonlinear, and therefore FDI should employ nonlinear algorithms, which are difficult to generalize and apply in many cases. It is well known that sliding mode techniques offer good potential for increasing the robustness of FDI by including a nonlinear discontinuous term that depends on the output estimation error into the observer [15-16]. During the last two decades, the research on sliding-mode observers (SMO)-based FE has received considerable attention. Several results have been reported on this topic [17-21].

Among various types of FE methods that have been developed, SMO-based FE has been proven to be an effective way to estimate/reconstruct faults for many systems [22-25]. These researches deal separately with actuator or sensor faults. However, in many practical systems, actuators and sensors are jointly prone to faults. Misinterpretation of actuator and sensor faults may cause a high rate of false alarm and unnecessary maintenance. Therefore, it would be desirable to consider actuator and sensor faults under a unified framework.

In this paper, an estimation fault scheme is considered for uncertain Lipschitz nonlinear systems that are subject to actuator and sensor faults simultaneously. The proposed schemes essentially transform the original system into two subsystems, where subsystem-1 includes the effects of actuator faults but is free from sensor faults and subsystem-2 only has sensor faults. Using an integral observer-based approach [26], sensor faults in subsystem-2 are transformed such that they appear as actuator faults. The augmented subsystem-2 is further transformed by a linear coordinate transformation such that a specific structure can be imposed to the sensor fault distribution matrix. In the first scheme, it is assumed that the fault distribution matrix satisfies the matching condition. Then two SMOs are designed to estimate actuator and sensor faults, respectively. However, this assumption is restrictive and sometimes it is difficult to find such matrices to satisfy both the Lyapunov equation and matching condition. To overcome the restriction imposed by the matching condition, many attempts have been made using high-order SMOs [27-28]. The sufficient conditions for the existence of the proposed observers with H∞ performance are derived and expressed as an LMI optimization problem such that the upper bounds of the state and fault estimation errors can be minimized.

The remainder of the paper is organized as follows: Section 2 briefly describe model of the steer-by-wire (SBW) vehicle under faults, disturbances and noise. Section 3 describes the mathematical preliminaries required for developing the FDI method and design procedure of the implemented SMO. The results of the simulation are shown in Section 4 and conclusions are given in Section 5.

2. DESCRIPTION OF THE SBW VEHICLE

Let's consider the following model of a steer-by-wire (SBW) vehicle subject to actuator and sensor faults, disturbances and measurement noise:

$$
\begin{aligned}
\dot{\beta}_s &= -\frac{c_0}{mu_x}\beta_s + \left(\frac{c_1}{mu_x^2}-1\right)\gamma_s + \frac{c_{\alpha f}}{mu_x}\left(\delta_s + f_a\right) + d \\
\dot{\gamma}_s &= -\frac{c_1}{I_z}\beta_s - \left(\frac{c_1}{I_z u_x}\right)\gamma_s + \frac{c_{\alpha f}a}{I_z}\left(\delta_s + f_a\right) + d \\
y_{01} &= \beta_s + w \\
y_{02} &= \gamma_s + f_s + w
\end{aligned}
\tag{1}
$$

with $c_0 = c_{\alpha f} + c_{\alpha r}$, $c_1 = c_{\alpha r}b - c_{\alpha f}a$, $c_{\alpha f}a^2 + c_{\alpha r}b^2$. The different parameters m, I_z, $c_{\alpha f}$, $c_{\alpha r}$, a and b are given with corresponding numerical values in Table 1. The slide-slip angle at the center of gravity is represented by β_s, γ_s is the yaw rate, δ_s is the front steering angle of the vehicle, and u_x represents the longitudinal velocity which is assumed constant and equal to 8 m/s. Also, $x_1 = \beta_s$ and $x_2 = \gamma_s$ are the state variables, $u = \delta_s$ is the control input of the system, f_a is the actuator fault, f_s is the sensor fault, d represents the disturbance corrupting the dynamics and w is the measurement noise.

Table 1. Parameters of the steer-by-wire vehicle model.

Notations	Denotes
$m = 350\ kg$	Mass of the vehicle
$I_z = 260\ kgm^2$	Moment of inertia of the front wheel system
$c_{\alpha f} = 2700\ N/rad$	Front cornering stiffness
$c_{\alpha r} = 2700\ N/rad$	Rear cornering stiffness
$a = 0.65\ m$	Distance from the center of gravity to the front axle
$b = 0.83\ m$	Distance from the center of gravity to the rear axle

3. JOINT ESTIMATION OF ACTUATOR AND SENSOR FAULTS USING SMO

Consider a non-linear system described by

$$\begin{aligned}\dot{x}(t) &= Ax(t) + f(x,t) + B\big(u(t) + f_a(t)\big) + E\Delta\psi(t)\\ y &= Cx(t) + Df_s(t)\end{aligned} \tag{2}$$

where the state vector is $x \in R^n$, the input vector is $u \in R^m$, the output vector is $y \in R^p$, the actuator fault is denoted as $f_a \in R^m$, the sensor fault is denoted as $f_s \in R^q$. The known constant matrices are $A \in R^{n\times n}$, $B \in R^{n\times m}$, $C \in R^{p\times n}$, $D \in R^{p\times q}$, $E \in R^{n\times r}$ (p ≥ q) and B and D both being of full rank.

Remark 1: It should be noted that the system uncertainty under consideration is unstructured, which is more general than the type of structured uncertainty that has been considered for fault diagnosis of Lipschitz nonlinear systems in the literature [30]. In the case of structured system uncertainty, certain rank conditions of the uncertainty distribution matrix are assumed to be satisfied such that the fault can be completely decoupled from the uncertainty.

For the objective of achieving fault diagnosis, the following assumptions and Lemmas are introduced. The nonlinear term $f(x,t) \in R^n$ is assumed to be known and Lipschitz about x uniformly $\forall x, \hat{x} \in R^n$.

$$\|f(x,t) - f(\hat{x},t)\| \le \mathrm{L}_{ff}\|x - \hat{x}\| \tag{3}$$

where L_{ff} is the known Lipschitz constant. The unknown nonlinear term $\Delta\psi(t)$ is structured modelling uncertainty, but bounded, and satisfies $\Delta\psi(t) \le \xi$. Also, the unknown sensor fault and its derivative are norm bounded, i.e. $f_s(t) \le \rho$ and $\dot{f}_s(t) \le \rho_s$.

Lemma 1. [30] Let's assume $\mathrm{rank}(CB) = \mathrm{rank}(B)$. There exist state and output transformations of coordinates

$$h = \begin{bmatrix} h_1 \\ h_2 \end{bmatrix} = Tx \text{ and } w = \begin{bmatrix} w_1 \\ w_2 \end{bmatrix} = Sy \tag{4}$$

such that in the new coordinates, the system matrices become

$$TAT^{-1} = \begin{bmatrix} A_1 & A_2 \\ A_3 & A_4 \end{bmatrix},\ TB = \begin{bmatrix} B_1 \\ 0 \end{bmatrix},\ TE = \begin{bmatrix} E_1 \\ E_2 \end{bmatrix},\ SCT^{-1} = \begin{bmatrix} C_1 & 0 \\ 0 & C_4 \end{bmatrix},\ SD = \begin{bmatrix} 0 \\ D_2 \end{bmatrix} \tag{5}$$

where $T \in R^{n\times n}$, $S \in R^{p\times p}$, $T_1 \in R^{m\times n}$, $S_1 \in R^{m\times p}$, $h_1 \in R^m$, $w_1 \in R^m$, $A_1 \in R^{m\times m}$, $A_4 \in R^{(n-m)\times(n-m)}$, $B_1 \in R^{m\times m}$, $E_1 \in R^{m\times r}$, $C_1 \in R^{m\times m}$, $C_4 \in R^{(p-m)\times(n-m)}$ and $D_2 \in R^{(p-m)\times q}$. B_1 and C_1 is invertible.

After introducing the state and output transformations (4), the original system is converted into two subsystems:

$$\text{Subsystem 1:} \begin{cases} \dot{h}_1 = A_1h_1 + A_2h_2 + T_1f(T^{-1}h,t) + B_1(u + f_a) + E_1\Delta\psi(t) \\ w_1 = C_1h_1 \end{cases} \tag{6}$$

$$\text{Subsystem 2:}\begin{cases}\dot{h}_2 = A_3h_1 + A_4h_2 + T_2f(T^{-1}h,t) + E_2\Delta\psi \\ w_2 = C_4h_2 + D_2f_s\end{cases} \tag{7}$$

For Subsystem 2, we define a new state $h_3 = \int_0^t w_2(\tau)d\tau$ so that $\dot{h}_3 = C_4h_2 + D_2f_s$. An augmented system with the new state h_3 is therefore given as:

$$\begin{aligned}&\dot{h}_0 = A_0h_0 + \bar{A}_3h_1 + \bar{T}_2f(T^{-1}h,t) + D_0f_s + E_0\Delta\psi \\ &w_3 = C_0h_0\end{aligned} \tag{8}$$

in which $h_0 = \begin{bmatrix}h_2 & h_3\end{bmatrix}^T \in R^{n+p-2m}$, $w_3 \in R^{p-m}$, $A_0 = \begin{bmatrix}A_4 & 0 \\ C_4 & 0\end{bmatrix} \in R^{(n+p-2m)\times(n+p-2m)}$, $\bar{A}_3 = \begin{bmatrix}A_3 \\ 0\end{bmatrix} \in R^{(n+p-2m)\times m}$, $E_0 = \begin{bmatrix}E_2 \\ 0\end{bmatrix} \in R^{(n+p-2m)\times r}$, $D_0 = \begin{bmatrix}0 \\ D_2\end{bmatrix} \in R^{(n+p-2r)\times q}$, $C_0 = \begin{bmatrix}0 & I_{p-m}\end{bmatrix} \in R^{(p-m)\times(n+p-2m)}$, $\bar{T}_2 = \begin{bmatrix}T_2 \\ 0\end{bmatrix} \in R^{(n+p-2m)\times n}$.

Lemma 2.[31-32] The pair (A_0, C_0) is observable if and only if the minimum phase condition holds

$$\operatorname{rank}\begin{bmatrix}sI_n - A & B \\ C & 0\end{bmatrix} = n + \operatorname{rank}(B) \tag{9}$$

for every complex number s with nonnegative real part.

Now, a scheme which consists of two SMOs to estimate actuator and sensor faults is developed. One SMO is designed to estimate actuator faults while the other one is designed to estimate sensor faults.

By taking the state transformation of $z \triangleq T_0h_0 = [z_1^T z_2^T]^T$ with

$$T_0 = \begin{bmatrix}I_{n-p} & P_{01}^{-1}P_{02} \\ 0 & I_{p-m}\end{bmatrix} \tag{10}$$

where $z_1 \in R^{n-m}$ and $z_2 \in R^{p-m}$.

Subsystem (8) can be rewritten as in a more compact form as

$$\begin{aligned}&\dot{z} = A_zz + T_0A_3h_1 + T_0\bar{T}_2f(T^{-1},t) + D_zf_s + E_z\Delta\psi \\ &w_3 = C_zz\end{aligned} \tag{11}$$

where

$$A_z = \begin{bmatrix}A_4 + P_{01}^{-1}P_{02}C_4 & -A_4P_{01}^{-1}P_{02} - P_{01}^{-1}P_{02}C_4P_{01}^{-1}P_{02} \\ C_4 & -C_4P_{01}^{-1}P_{02}\end{bmatrix},\ D_z = \begin{bmatrix}P_{01}^{-1}P_{02}D_2 \\ D_2\end{bmatrix},\ E_z = \begin{bmatrix}E_2 \\ 0\end{bmatrix},\ C_z = [0 \quad I_{p-m}] \tag{12}$$

Lemma 3.[31][32] If there exists an arbitrary matrix $F_0 \in R^{q(p-m)}$ such that

$$D_0^TP_0 = F_0C_0 \tag{13}$$

then we have

$$P_{02}D_2 = 0\,, \tag{14}$$

$$F_0 = D_2^T\bar{P}_{03}\,. \tag{15}$$

Therefore, Systems (6) and (11) can be rewritten respectively as

$$\text{Subsystem 1:}\begin{cases}\dot{h}_1 = A_1h_1 + A_2z_1 + A_2P_{01}^{-1}P_{02}w_3 + T_2f(T^{-1}h,t) + B_1(u+f_a) + E_1\Delta\psi(t) \\ w_1 = C_1h_1\end{cases} \tag{16}$$

$$\text{Subsystem 2}:\begin{cases}\dot{z}_1=\bar{A}_1z_1+\bar{A}_2z_2+A_3h_1+T_2f(T^{-1}h,t)+E_2\Delta\psi\\ \dot{z}_2=\bar{A}_3z_1+\bar{A}_4z_2+D_2f_s\\ w_3=z_2\end{cases} \tag{17}$$

For the above systems it is constructed the following two SMOs:

$$\begin{cases}\dot{\hat{h}}_1=A_1\hat{h}_1+A_2\hat{z}_1-A_2P_{01}^{-1}P_{02}w_3+T_2f(T^{-1}\hat{h},t)+B_1(u+v_1)+(A_1-A_{1s})C_1^{-1}(w_1-\hat{w}_1)\\ \hat{w}_1=C_1\hat{h}_1\end{cases} \tag{18}$$

$$\begin{cases}\dot{\hat{z}}_1=\bar{A}_1\hat{z}_1+\bar{A}_2w_3+A_3C_1^{-1}w_1+T_2f(T^{-1}\hat{h},t)\\ \dot{\hat{z}}_2=\bar{A}_3\hat{z}_1+\bar{A}_4\hat{z}_2+(\bar{A}_4-L)(\bar{w}_3-w_3)+D_2v_2\\ \hat{w}_3=\hat{z}_2\end{cases} \tag{19}$$

where $\hat{h}_1,\hat{z}_1,\hat{z}_2,\hat{w}_1$ and $\hat{w}_3$ denote, respectively, the estimated h_1,z_1,z_2,w_1 and w_3. $A_1^s\in R^{m\times m}$ is a stable matrix, and $L\in R^{(p-m)\times(p-m)}$ is the observer gain. It is worth noting that $\hat{h}\triangleq \mathrm{col}(C_1^{-1}S_1y,\ \hat{z}_1-P_{01}^{-1}P_{02}w_3)$ and does not represent the state estimate vector $\mathrm{col}(\hat{h}_1,\hat{h}_2)$. The discontinuous output error injection terms v1 and v2 are defined by

$$v_1=\begin{cases}(\rho_a+\eta_1)\dfrac{B_1^TP_1\left(C_1^{-1}S_1y-\hat{h}_1\right)}{\left\|B_1^TP_1\left(C_1^{-1}S_1y-\hat{h}_1\right)\right\|}, & C_1^{-1}S_1y-\hat{h}_1\neq 0\\ 0 & \text{otherwise}\end{cases} \tag{20}$$

$$v_2=\begin{cases}(\rho_s+\eta_2)\dfrac{D_2^T\bar{P}_{03}\left(w_3-\hat{w}_3\right)}{\left\|D_2^T\bar{P}_{03}\left(w_3-\hat{w}_3\right)\right\|}, & w_3-\hat{w}_3\neq 0\\ 0 & \text{otherwise}\end{cases} \tag{21}$$

where $P_1\in R^{m\times m}$ is the symmetric definite Lyapunov matrix for A_1^s, and η_1 and η_2 are two positive scalars which are to be determined.

If the state estimation errors are defined as $e_1=h_1-\hat{h}_1$, $e_2=z_1-\hat{z}_1$, and $e_3=z_2-\hat{z}_2$ then the controlled estimation error can be obtained as

$$r=He=H\begin{bmatrix}e_1\\ e_2\\ e_3\end{bmatrix} \tag{22}$$

We now present Theorem 1 which establishes the sufficient conditions for the existence of the proposed SMOs in the form of (18) and (19) with a prescribed performance

$$\|H\|_\infty \triangleq \sup_{\|\Delta\psi\|_{L_2}\neq 0}\frac{\|r\|_{L_2}^2}{\|\Delta\psi\|_{L_2}^2}\leq\mu, \tag{23}$$

where μ is a small positive constant.

Theorem 1. Let's consider system (2) with introduced lemmas. If there exist matrices A_1^s, L, $P_1=P_1^T>0$, $P_{01}=P_{01}^T>0$, $P_{03}=P_{03}^T>0$, and P_{02}, and positive scalars α_1, α_2 and μ such that

$$P_{02}D_2=0 \tag{24}$$

$$\Lambda\triangleq\begin{bmatrix}\Pi_1+H_1^TH_1 & P_1A_2 & 0 & P_1E_1\\ A_2^TP_1 & \Pi_2+H_2^TH_2 & C_4^T\bar{P}_{03} & P_{01}E_2\\ 0 & \bar{P}_{03}C_4 & \Pi_3+H_3^TH_3 & 0\\ T_1^TP_1 & T_2^TP_{01} & 0 & -\mu I_r\end{bmatrix}<0 \tag{25}$$

where $\Pi_1 = A_1^{sT}P_1 + P_1A_1^s + \frac{1}{\alpha_1}P_1T_1T_1^TP_1$, $\Pi_2 = A_4^TP_{01} + P_{01}A_4 + C_4^TP_{02}^T + P_{02}C_4 + \frac{1}{\alpha_2}P_{01}T_2T_2^TP_{01} + (\alpha_1+\alpha_2)\mathrm{L}_f^2\left\|T^{-1}\right\|^2 I_{n-m}$ and $\Pi_3 = \bar{P}_{03}L + L^T\bar{P}_{03}$, then the estimation error dynamics are asymptotically stable with the prescribed H_∞ tracking performance $\|r\|_{\mathrm{L}_2} \le \sqrt{\mu}\|\Delta\psi\|_{\mathrm{L}_2}$. The Proof of Theorem 1 can be seen in [33].

Theorem 2. Let's consider system (2) with introduced lemmas. If there exist matrices A_1^s, X, Y, Z, $P_1 = P_1^T > 0$, $P_{01} = P_{01}^T > 0$, $P_{03} = P_{03}^T > 0$, and positive scalars α_1, α_2 such that the following LMI feasibility problem has a solution:

$$\begin{bmatrix} X + X^T + H_1^TH_1 & P_1A_2 & 0 & P_1E_1 & P_1T_1 & 0 \\ A_2^TP_1 & \Pi_4 + H_2^TH_2 & C_4^T\bar{P}_{03} & P_{01}E_2 & 0 & P_{01}T_2 \\ 0 & \bar{P}_{03}C_4 & Y + Y^T + H_3^TH_3 & 0 & 0 & 0 \\ E_1^TP_1 & E_2^TP_{01} & 0 & -\mu I & 0 & 0 \\ T_1^TP_1 & 0 & 0 & 0 & -\alpha_1 I & 0 \\ 0 & T_2^TP_{01} & 0 & 0 & 0 & -\alpha_2 I \end{bmatrix} < 0 \tag{26}$$

where

$$\Pi_4 = A_4^TP_{01} + P_{01}A_4 + (\alpha_1+\alpha_2)\mathrm{L}_f^2\left\|T^{-1}\right\|^2 I_{n-m} + ZC_4 - ZD_2D_2^+C_4 + (ZC_4)^T - (ZD_2D_2^+C_4)^T$$

then the estimation error dynamics is asymptotically stable with the prescribed H_∞ tracking performance $\|r\|_{\mathrm{L}_2} \le \sqrt{\mu}\|\Delta\psi\|_{\mathrm{L}_2}$. The Proof of Theorem 2 can be seen in [33].

The effect of system uncertainties on the estimation errors is decided by the value of μ. The accuracy of the fault estimation increases with smaller value of μ. The minimization of μ can be found by solving the following LMI optimization problem:

$$\begin{aligned} &\text{minimize } \mu \text{ subject to} \\ &X < 0,\ P_1 > 0,\ P_{01} > 0,\ \bar{P}_{03} > 0 \text{ and (26).} \end{aligned} \tag{27}$$

We have proved that the proposed observers are asymptotically stable with the prescribed H_∞ performance in Theorem 2. The objective now is to determine the constant gain η_1 in (20) and η_2 in (21) such that the error systems can be directed to the sliding surface S which is defined as

$$\mathrm{S} = \left\{(e_1, e_2, e_3) \middle| e_1 = 0,\ e_3 = 0\right\} \tag{28}$$

in finite time and maintain on it thereafter.

Theorem 3. Let's consider system (2) with introduced assumptions, lemmas and the proposed observers (18) and (19). Then the error dynamics

$$\dot{e}_1 = A_1^se_1 + A_2e_2 + T_1\left(f(T^{-1}h,t) - f(T^{-1}\hat{h},t)\right) + B_1\left(f_a - v_1\right) + E_1\Delta\psi \tag{29}$$

$$\dot{e}_2 = \bar{A}_1e_2 + T_2\left(f(T^{-1}h,t) - f(T^{-1}\hat{h},t)\right) + E_2\Delta\psi \tag{30}$$

$$\dot{e}_3 = \bar{A}_3e_2 + Le_3 + D_2\left(f_s - v_2\right) \tag{31}$$

can be driven to the sliding surface (28) in finite time and remain on it if LMI optimization problem formulated in (27) is solvable and the gains η_1 and η_2 satisfy

$$\eta_1 \ge \left\|B_1^{-T}\right\|\left(\|A_2\|\|e_2\| + \mathrm{L}_f\|T_1\|\left\|T^{-1}\right\|\|e_2\| + \|E_1\|\xi\right) + \eta_3, \tag{32}$$

$$\eta_2 \ge \frac{\|C_4e_2\| + \eta_4}{\left\|D_2^T\bar{P}_{03}e_3\right\|}, \tag{33}$$

where η_3 and η_4 are positive scalars. The Proof of Theorem 3 can be seen in [33].

Given the observers in the form of (18) and (19), the objective now is to simultaneously estimate actuator and sensor faults. From Theorem 3, we know that an ideal sliding motion (28) will take place after some finite time if the conditions (32) and (33) are satisfied. During the sliding motion, (29) becomes

$$0 = A_2 e_2 + T_1\left(f(T^{-1}h,t) - f(T^{-1}\hat{h},t)\right) + B_1\left(f_a - v_{1eq}\right) + E_1 \Delta\psi \tag{34}$$

where v_{1eq} is the equivalent output error injection signal to maintain the sliding motion [33], and can be approximated to any degree of accuracy by replacing (20) with

$$v_1 \approx \left(\rho_a + \eta_1\right) \frac{B_1^T P_1\left(C_1^{-1} S_1 y - \hat{h}_1\right)}{\left\| B_1^T P_1\left(C_1^{-1} S_1 y - \hat{h}_1\right)\right\| + \delta_1} \tag{35}$$

where δ_1 is a small positive scalar to reduce the chattering effect.

Since B_1 is invertible, (34) can be further rewritten as

$$f_a - v_{1eq} = -B_1^{-1}\left(A_2 e_2 + T_1\left(f(T^{-1}h,t) - f(T^{-1}\hat{h},t)\right)\right) + E_1 \Delta\psi \tag{36}$$

Computing the L_2 norm of (36) yields

$$\begin{aligned} \left\| f_a - v_{1eq} \right\|_{\mathrm{L}_2} &= \left\| B_1^{-1}\left(A_2 e_2 + T_1\left(f(T^{-1}h,t) - f(T^{-1}\hat{h},t)\right)\right) + E_1 \Delta\psi \right\|_{\mathrm{L}_2} \le \left(\sigma_{max}\left(B_1^{-1}A_2\right) + \sigma_{max}\left(B_1^{-1}T_1\right)\mathrm{L}_f \left\|T^{-1}\right\|\right)\|e\|_{\mathrm{L}_2} + \\ &+ \sigma_{max}\left(B_1^{-1}E_1\right)\|\Delta\psi\|_{\mathrm{L}_2} \end{aligned} \tag{37}$$

Since $\|e\|_{\mathrm{L}_2} \le \sigma_{max}\left(H^{-1}\right)\sqrt{\mu}\|\Delta\psi\|_{\mathrm{L}_2}$, it can be obtained that

$$\left\| f_a - v_{1eq} \right\|_{\mathrm{L}_2} = \left(\sqrt{\mu}\left(\sigma_{max}\left(B_1^{-1}A_2\right) + \sigma_{max}\left(B_1^{-1}T_1\right)\mathrm{L}_f \left\|T^{-1}\right\|\right)\right) \cdot \sigma_{max}\left(H^{-1}\right) + \sigma_{max}\left(B_1^{-1}E_1\right)\|\Delta\psi\|_{\mathrm{L}_2} \tag{38}$$

It follows that

$$\sup_{\|\Delta\psi\|_{\mathrm{L}_2} \ne 0} \frac{\left\| f_a - v_{1eq} \right\|_{\mathrm{L}_2}}{\|\Delta\psi\|_{\mathrm{L}_2}} \le \mu\beta_1 + \beta_2, \tag{39}$$

where $\beta_1 = \left(\sigma_{max}\left(B_1^{-1}A_2\right) + \sigma_{max}\left(B_1^{-1}T_1\right)\mathrm{L}_f \left\|T^{-1}\right\|\right)\sigma_{max}\left(H^{-1}\right)$ and $\beta_2 = \sigma_{max}\left(B_1^{-1}E_1\right)$.

Thus for a small $\left(\mu\beta_1 + \beta_2\right)\|\Delta\psi\|_{\mathrm{L}_2}$, the actuator faults f_a can be approximated as

$$\hat{f}_a \approx \left(\rho + \eta_1\right) \frac{B_1^T P_1\left(C_1^{-1} S_1 y - \hat{h}_1\right)}{\left\| B_1^T P_1\left(C_1^{-1} S_1 y - \hat{h}_1\right)\right\| + \delta_1} \tag{40}$$

Similarly, we can get that

$$\sup_{\|\Delta\psi\|_{\mathrm{L}_2} \ne 0} \frac{\left\| f_a - v_{2eq} \right\|_{\mathrm{L}_2}}{\|\Delta\psi\|_{\mathrm{L}_2}} \le \sqrt{\mu}\sigma_{\max}\left(H^{-1}\right)\sigma_{\max}\left(D_2^{+}\bar{A}_3\right) \tag{41}$$

where v_{2eq} is the equivalent output error injection signal which can be approximated as

$$v_2 \approx \left(\rho_s + \eta_2\right) \frac{D_2^T \bar{P}_{03}\left(w_3 - \hat{w}_3\right)}{\left\| D_2^T \bar{P}_{03}\left(w_3 - \hat{w}_3\right)\right\| + \delta_2} \tag{42}$$

where δ_2 is a small positive scalar. Thus for a small $\sqrt{\mu}\sigma_{\max}\left(H^{-1}\right)\sigma_{\max}\left(D_2^{+}\bar{A}_3\right)\|\Delta\psi\|_{\mathrm{L}_2}$, the sensor faults f_s can be approximated as

$$\hat{f}_s \approx \left(\rho_s + \eta_2\right) \frac{D_2^T \bar{P}_{03}\left(w_3 - \hat{w}_3\right)}{\left\| D_2^T \bar{P}_{03}\left(w_3 - \hat{w}_3\right)\right\| + \delta_2}. \tag{43}$$

4. SIMULATION RESULTS

It is assumed that there is a complex sensor fault composed of a combination of abrupt, ramp, and sine-type faults, which is represented as:

$$f_s = \begin{cases} 0 & t < 50 \\ 0.05 \cdot \sin(0.15\pi t) & 50 \le t < 90 \\ 0 & 90 \le t < 100 \end{cases}, \tag{44}$$

$$f_a = \begin{cases} 0 & t < 20 \\ 0.2 \cdot (t - 20) & 20 \le t < 50 \\ 0.5 + 0.2 \cdot \sin(0.2\pi t) & 50 \le t < 100 \end{cases}. \tag{45}$$

For simulation purposes, we set the control input $u(t)$ as sinus function $\sin(\pi t)$ and the system uncertainty $\Delta\psi(t)$ as

$$\Delta\psi(t) = \begin{bmatrix} 0.1\sin(0.2t)^2 \\ 0.1\sin(0.1t)^2 \\ 0.2\sin(t)^2 \\ 0.3\sin(t)^2 \end{bmatrix}. \tag{46}$$

The results of sensor and actuator faults estimation are illustrated in Fig.1 and Fig.2. These figures clearly demonstrate that the proposed SMO based estimation method is able to estimate the faults successfully, irrespective of uncertainties in the system. In addition to gradual and slow faults, such as a ramp and sinusoidal faults, it should be noted that f_a changes abruptly at time instant 50s, which indicates that the proposed approach has the ability to track abrupt faults.

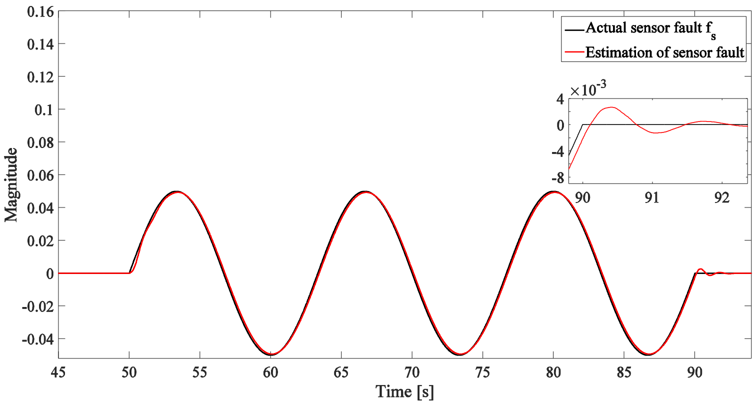

Figure 1: Estimation of the sensor fault

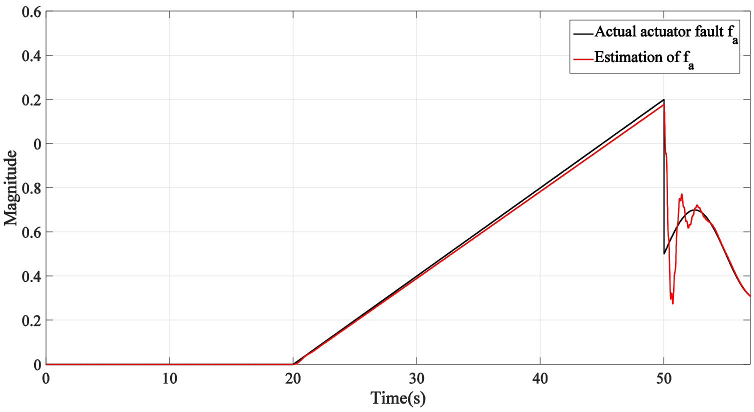

Figure 2: Estimation of the actuator fault

Fig. 3 shows the trajectories of the actual states and their estimates. It can be seen from the figures that the proposed SMO approach can estimate the states accurately, before and after the occurrence of any fault.

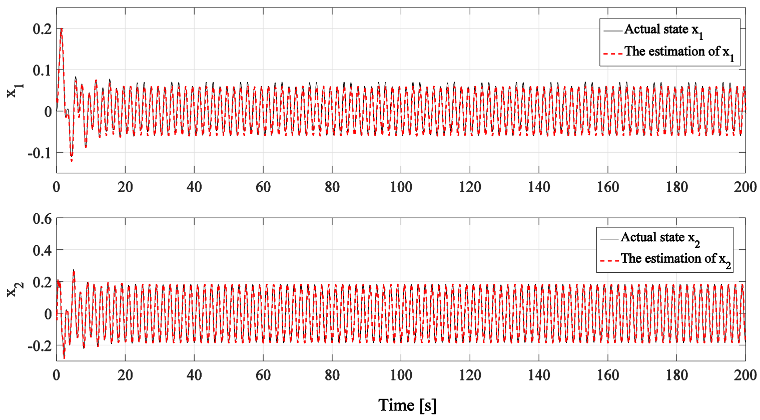

Figure 3: System states and their estimates

It can be seen that despite the presence of system uncertainties and measurement noises, the tracking performances of states x and actuator and sensor fault have achieved an ideal performance.

5. CONCLUSIONS

In this paper, an algorithm for jointly estimating actuator and sensor faults for uncertain Lipschitz nonlinear systems is considered. The proposed method uses two SMOs and can effectively estimate both the actuator and sensor faults provided certain matching condition is satisfied. Moreover, H∞ filtering is integrated into the algorithm to attenuate the effects of the system uncertainties on state and fault estimates. The simulation results show that proposed approach can successfully estimate actuator and sensor faults simultaneously despite the existence of system uncertainties. When the outputs are contaminated by noises, sensor fault estimates can still be obtained. However, real-world applications are not focused exclusively on successful FE. When a system is subject to a set of possible faults, fault-tolerant control (FTC) is necessary to maintain stability and reliability. We will study this issue in future.

ACKNOWLEDGEMENTS

This research has been supported by the Serbian Ministry of Education, Science and Technological Development under grant 451-03-68/2022-14/200108, and CNPq under grant 304032/2019-0.

REFERENCES

[1] Zhang, J., A. K. Swain, and S. K. Nguang, "Detection and isolation of incipient sensor faults for a class of uncertain nonlinear systems", IET Contr. Theory Appl., Vol. 6, pp. 1870–1880, https://doi.org/10.1049/iet-cta.2011.0440, (2012).

[2] Zhang, P. and J. Zou, "Observer-based fault diagnosis and self-restore control for systems with measurement delays", Asian J. Control, Vol. 14, pp. 1717–1723, https://doi.org/10.1002/asjc.458, (2012)

[3] Jayamaha DK, Lidula NW, Rajapakse AD "Wavelet-multi resolution analysis based ANN architecture for fault detection and localization in DC microgrids", IEEE Access, Vol.3(7), pp. 145371–84, https://doi.org/10.1109/ACCESS.2019.2945397, (2019)

[4] Z. Wang, Y. Shen, X. Zhang, "Actuator fault estimation for a class of nonlinear descriptor systems", Int J Syst Sci, Vol.45, pp. 487–496, https://doi.org/10.1080/00207721.2012.724100, (2014).

[5] J. Yang, Y. Guo, W. Zhao, "Long short-term memory neural network based fault detection and isolation for electro-mechanical actuators", Neurocomputing, Vol. 360, pp. 85–96, https://doi.org/10.1016/j.neucom.2019.06.029, (2019).

[6] F. Ferracuti, V. Artists, A. Monteriù, "Algorithms for Fault Detection and Diagnosis", MDPI AG, Basel, Switzerland, https://doi.org/10.3390/books978-3-0365-0463-6, (2021).

[7] S. Gómez-Peñate, G. Valencia-Palomo, FR. López-Estrada, CM. Astorga-Zaragoza, R.A. Osornio-Rios, I. Santos-Ruiz, "Sensor fault diagnosis based on a sliding mode and unknown input observer for Takagi-Sugeno systems with uncertain premise variables", Asian J Control, Vol. 21(1), pp. 339-353, https://doi.org/10.1002/asjc.1913, (2019).

[8] D. Henry, J. Cieslak, A. Zolghadri, D. Efimov, "H∞/ H-LPV solutions for fault detection of aircraft actuator faults: bridging the gap between theory and practice", Int J Robust Nonlinear Control, Vol.25(5), pp. 649-672, https://doi.org/10.1002/rnc.3157, (2015).

[9] Q. Jia, W. Chen, Y. Zhang, X. Chen, "Robust fault reconstruction via learning observers in linear parameter-varying systems subject to loss of actuator effectiveness", IET Control Theory Appl, Vol. 8(1), pp. 42-50, https://doi.org/10.1049/iet-cta.2013.0417, (2014).

[10] D. Rotondo, A. Cristofaro, T.A. Johansen, F. Nejjari, V. Puig, "Robust fault and icing diagnosis in unmanned aerial vehicles using LPV interval observers", Int J Robust Nonlinear Control, Vol. 29(16), pp. 5456-5480, https://doi.org/10.1002/rnc.4381, (2019).

[11] S. Li, H. Wang, A. Aitouche, N. Christov, "Unknown input observer design for faults estimation using linear parameter varying model. application to wind turbine systems", Paper presented at: Proceedings of the 2018 7th International Conference on Systems and Control, Valencia, Spain, pp. 45-50, https://doi.org/10.1109/ICoSC.2018.8587778, (2018).

[12] J. Zhang, A.K. Swain, S.K. Nguang, "Robust sliding mode observer based fault estimation for certain class of uncertain nonlinear systems", Asian Journal of Control, https://doi.org/10.1002/asjc.987, (2015).

[13] C. Bonivento, A. Isidoria, L. Marconia, A. Paolia, "Implicitfault-tolerant control: application to induction motors", Automatica, Vol.40(3), pp. 355–371, https://doi.org/10.1016/j.automatica.2003.10.003, (2004).

[14] Z.W. Gao, S.X. Ding, "Sensor fault reconstruction and sensor compensation for a class of nonlinear state-space systems via a descriptor system approach", IET Control Theory Appl, Vol.1, pp. 578–585, https://doi.org/10.1049/iet-cta:20050509, (2007).

[15] C.P. Tan, C. Edwards, "An LMI approach for designing sliding mode observers", Int J Control, Vol. 74(16), pp. 1559-1568, https://doi.org/10.1080/00207170110081723, (2001).

[16] VI. Utkin, "Sliding Modes in Control and Optimization", Berlin, Germany, Springer Science & Business Media, https://doi.org/10.1007/978-3-642-84379-2, (2013).

[17] C.P. Tan, C. Edwards, "Sliding mode observers for detection and reconstruction of sensor faults", Automatica, Vol. 38, pp. 1815–1821, https://doi.org/10.1016/S0005-1098(02)00098-5, (2002).

[18] B. Jiang, M. Staroswiecki, V. Cocquempot, "Fault estimation in nonlinear uncertain systems using robust/sliding-mode observers", IEE Proc Control Theory Appl, Vol. 151(1), pp. 29–37, https://doi.org/10.1049/ip-cta:20040074, (2004).

[19] F.E. Thomas, I. Castillo, R.F. Benito, "Robust model-based fault detection and isolation for nonlinear processes using sliding modes", Int J Robust Nonlinear Control, Vol. 22, pp. 89–104, https://doi.org/10.1002/rnc.1807 (2012).

[20] CP. Tan, C. Edwards, "Sliding mode observers for robust detection and reconstruction of actuator and sensor faults", Int J Robust Nonlinear Control, Vol. 13, pp. 443–463, https://doi.org/10.1002/rnc.723, (2003).

[21] C.P. Tan, C. Edwards, "A robust sensor fault tolerant control scheme implemented on a crane", Asian J Control, Vol. 9(3), pp. 340–344, https://doi.org/10.1111/j.1934-6093.2007.tb00420.x, (2007).

[22] C. Edwards, S.K. Spurgeon, R.J. Patton, "Sliding mode observers for fault detection and isolation", Automatica, Vol. 36, pp. 541–553, https://doi.org/10.1016/S0005-1098(99)00177-6, (2000).

[23] X.G. Yan, C. Edwards, "Sensor fault detection and isolation for nonlinear systems based on a sliding mode observer", Int J Adapt Control Signal Process, Vol. 21, pp. 657–673, https://doi.org/10.1002/acs.967, (2007).

[24] H. Alwi, C. Edwards, C.P. Tan, "Sliding mode estimation schemes for incipient sensor faults", Automatica, Vol. 45, pp.1679–1685, https://doi.org/10.1016/j.automatica.2009.02.031, (2009).

[25] X.G. Yan, C. Edwards, "Robust sliding mode observer-based actuator fault detection and isolation for a class of nonlinear systems", Int J Syst Sci, Vol. 39(4), pp. 349–359, https://doi.org/10.1080/00207720701778395, (2008).

[26] J. Zhang, A.K. Swain, S.K. Nguang, "Detection and isolation of incipient sensor faults for a class of uncertain nonlinear systems", IET Control Theory Appl, Vol. 6, pp. 1870–1880, https://doi.org/10.1049/iet-cta.2011.0440, (2012).

[27] T. Floquet, C. Edwards, S.K. Spurgeon, "On sliding mode observers for systems with unknown inputs", Int J Adapt Control Signal Process, Vol. 21, pp. 638–656, https://doi.org/10.1002/acs.958, (2007).

[28] F. Zhu, "State estimation and unknown input reconstruction via both reduced-order and high-order sliding mode observers", J Process Control, Vol. 22, 296–302, https://doi.org/10.1016/j.jprocont.2011.07.007, (2012)

[29] M. Jelali, A. Kroll, "Hydraulic Servo-systems: Modelling, Identification and Control", Berlin: Springer; https://doi.org/10.1007/978-1-4471-0099-7, (2003).

[30] R. Raoufi, H.J. Marquez, A.S.I. Zinober, "H∞ sliding mode observer for uncertain nonlinear Lipschitz systems with fault estimation synthesis", Int J Robust Nonlinear Control, Vol. 20, pp.1785–1801, https://doi.org/10.1002/rnc.1545, (2010).

[31] M. Corless, J. Tu, "State and input estimation for a class of uncertain systems", Automatica, Vol. 34, pp. 757–764, https://doi.org/10.1016/S0005-1098(98)00013-2, (1998).

[32] S. Hui, S.H. Zak, "Observer design for system with unknown inputs", Int. J. Appl. Math. Comput. Sci, Vol.15(4), pp. 431–446, (2005).

[33] J. Zhang, A.K. Swain, S.K. Nguang, "Robust Observer-Based Fault Diagnosis for Nonlinear Systems Using MATLAB®", Springer International Publishing, Switzerland, https://doi.org/10.1007/978-3-319-32324-4, (2016).

[34] Z.W. Gao, S.X. Ding, "Sensor fault reconstruction and sensor compensation for a class of nonlinear state-space systems via a descriptor system approach", IET Control Theory Application, Vol. 1, pp. 578–585, https://doi.org/10.1049/iet-cta:20050509, (2007).

[35] C. Gao, Q. Zhao, G. Duan, "Robust actuator fault diagnosis scheme for satellite attitude control systems", J Frankl Inst, Vol. 350(9), pp, 2560–2580, https://doi.org/10.1016/j.jfranklin.2013.02.021, (2013).

[36] F. Zhu, Z. Han, "A note on observers for lipschitz nonlinear systems", IEEE Trans Autom Control, Vol. 47, pp.1751–1754, https://doi.org/10.1109/TAC.2002.803552, (2002)

ORIGINAL SCIENTIFIC PAPER OPEN ACCESS

Metaheuristic Applications in Mechanical and Structural Design

Goran Pavlović[1*], Boris Jerman[2], Mile Savković[3], Nebojša Zdravković[3], Goran Marković[3]

[1] University of Niš, Faculty of Electronic Engineering, Niš, Serbia

[2] University of Ljubljana, Faculty of Mechanical Engineering, Ljubljana, Slovenia

[3] University of Kragujevac, Faculty of Mechanical and Civil Engineering in Kraljevo, Kraljevo, Serbia

ARTICLE INFO

* **Correspondence:** goran.pavlovic@elfak.ni.ac.rs

DOI: 10.5937/engtoday2201019P

UDC: 621(497.11) **ISSN:** 2812-9474

Article history: Received 24 February 2022; Accepted 30 March 2022

ABSTRACT

The paper shows the significance of metaheuristic optimization algorithms through their application to specific engineering problems, especially in mechanical and civil engineering domains, where some significant publications are presented. Moreover, due to their nature, these algorithms are very convenient for application in various engineering examples, both with single-objective or multi-objective optimization problems. Also, they are successfully being applied for tasks with a great number of variables and constraint functions. Finally, the paper presents the comparison of the results of seven chosen metaheuristic optimization algorithms that were applied on the example of the cantilever beam subjected to complex loading. The objective function was the cross-sectional area of the welded I-profile. In contrast, the constraint functions were the permissible stresses in the I-profile and the welded connection supporting a cantilever beam and one welding technology limitation. After comparing obtained optimum results, optimization time and convergence for all seven chosen algorithms, some conclusions and recommendations for an appropriate type choice and application were made.

KEYWORDS

Metaheuristic, Optimization, Bi-moment, Restrained warping, Cantilever beam, Mechanical design, Structural design

1. INTRODUCTION

Metaheuristic algorithms gain more and more appliances in optimization, especially in constrained engineering problems. Recent years have seen many bio-inspired metaheuristic algorithms emerge. Their application is frequent in various engineering problems, both with single-objective or multi-objective optimization problems, due to the possibility of managing many variables and constraint functions.

Metaheuristic algorithms are very efficient, and they don't require recalculations of derivatives of the objective function (which is required for the gradient optimization methods). The initial values of variables can be set within pretty wide bounds. The designer doesn't have to be experienced in setting the initial values of variables (which is very important). Metaheuristic algorithms can generate new solutions that are better in comparison to the previous ones and are very successfully avoiding the trap of entering a local optimum.

These algorithms are being applied in everyday research, so many research papers present their utilisation in the mechanical and civil engineering domain [1-20].

An improved new swarm intelligence optimization algorithm named the Multi-Specular Reflection Algorithm (M-SRA) is utilised in [1] to optimize the main girder of the double-beam bridge crane concerning lightweight and green design. The optimization of the main girder of the single-beam bridge crane is conducted in [2] by Bat Algorithm (BA), Cuckoo Search (CS) algorithm, and Firefly Algorithm (FA). Significant savings were achieved in relation to previous solutions, where the algorithm with the best results was revealed. Two algorithms inspired by laws of physics - Charged System Search (CSS) algorithm and Thermal Exchange Optimization (TEO) algorithm – were used in the optimization of cross-sections of the crane hook [3], where two cross-section types were considered. Again, significant savings were achieved in comparison with present solutions. Besides the mentioned mechanical engineering problems, these algorithms were successfully used for solving: gear train design problem [4-8], welded beam design problem [4, 5, 7-13], pressure vessel design problem [4, 5, 9, 11-13], tension/compression spring design problem [4, 7-13], cantilever beam design problem [4-6, 10], speed reducer design problem and rolling element bearing design problem [11, 12]. There was a comparison of applied algorithms and obtained results for each problem.

In addition, some of the metaheuristic algorithms are used in conjunction with Computational Fluid Dynamic (CFD) analysis for solving the airfoil design problem [10], using Salp Swarm Algorithm (SSA). In the same article, the mentioned algorithm was also used for multi-objective optimization in the marine propeller design problem. Furthermore, Sine Cosine Algorithm (SCA) was used for multi-objective optimization in the airfoil design problem [14]. The propeller design issue was considered as a single-objective optimization problem for efficiency increase [4, 6]. However, the submarine propeller design problem [15] was subject to multi-objective optimization by Dragonfly Algorithm (DA).

Besides mechanical design problems, these algorithms are frequently utilised in structural engineering. For example, [4, 10] considers the I-beam design problem, while [4-6, 10] studies the 3-bar truss design problem. In addition, the truss optimization problem has much research on it: 15-bar and 52-bar truss design problems were studied in [4, 9], 25-bar truss design problem (the base of transmission tower) was considered in [9, 11, 12, 16], and 72-bar truss design problem was addressed in [16, 17]. Again, there was a comparison of applied algorithms and obtained results for each problem.

Research [16] optimized the 120-bar dome truss structure and the planar 200-bar truss structure by Cyclical Parthenogenesis Algorithm (CPA). Also, the tower truss design problem (582-bar truss design problem) was solved by Enhanced Vibrating Particles System (EVPS) algorithm, [17]. The application of various technics and metaheuristic algorithms on many structural design problems and general engineering problems was presented in [18].

Authors in [19] presented the procedure of optimization for the steel girders in a high strength steel composite bridge from the viewpoint of weight, material cost and environmental impact. The Genetic Algorithm (GA) was used to solve this problem. Research [20] considered the problem of optimal design of buckling-restrained braced frames by using SSA and Enhanced Colliding Bodies Optimization (ECBO) algorithm.

So, the application of these algorithms is massive for various engineering problems. Besides showing these applications, especially in mechanical and civil engineering domains, this research aims to compare the results of more metaheuristic optimization algorithms applied to one specific engineering problem and give some directions about the choice of algorithm and its implementation.

2. APPLICATION OF METAHEURISTIC OPTIMIZATION ALGORITHMS

This research uses a welded I-section cantilever beam with fixed support [21] as an example of the engineering structure upon which the metaheuristic algorithms will be applied. The beam is subjected to torsion (M_z), axial eccentric force (F_z) and bending moment (M_{y1}), as depicted in Figure 1.

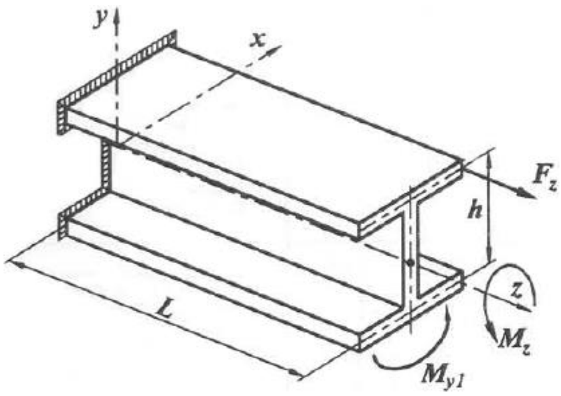

Figure 1: A cantilever beam

The goal of optimization is the reduction of the cross-sectional area of the welded I-profile. This single-objective multi-criteria optimization problem is a constrained optimization problem, and it is defined in the following way:

$$\min F(X) = f(X) + P(X, k_i) \tag{1}$$

$$P(X, k_i) = \sum_{i=1}^{n_g} k_i \cdot \left[\max\left(0, g_i(X)\right)\right]^2 \tag{2}$$

where *f (X)* is the objective function, *X* is the vector made of design variables, *P (X, k_i)* are the penalty functions, k_i are the penalty factors, $g_i(X)$ are the constraint functions, and n_g is the total number of constraint functions.

Variables (x_j) are defined by their lower (l_j) and upper bounds (u_j). This research treats five variables (Figure 2).

The objective function and constraint functions are presented in the following chapters (Chapter 2.1 and Chapter 2.2).

2.1. The Objective Function

The cross-sectional area (A_p) of the welded I-profile (the cross-sectional area of plates) represents the objective function *f(X)* in this optimization problem (Figure 2). The area of the welded connection ($A_š$) in support of a cantilever beam depends on this area (A_p).

The objective function is defined as follows:

$$f(X) = A_p = 2 \cdot b \cdot t + h \cdot d \tag{3}$$

All important geometric quantities are marked and defined, as shown in Figure 2.

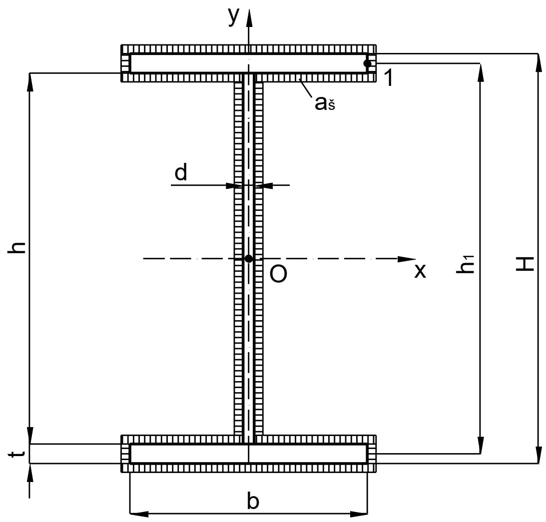

Figure 2: The cross-sectional area of the welded I-profile

The variables in this optimization process are:

$x_1 = b$ - the flange width, $x_2 = h$ - the web height, $x_3 = t$ - the flange thickness, $x_4 = d$ - the web thickness, and $x_5 = a_š$ - the weld thickness.

2.2. The Constraint Functions

In addition to the bending and tensile stresses that occur in the I-profile and the welded connection in support of a cantilever beam, stresses due to the restrained warping are also presented (Figure 1).

The maximum stresses due to the restrained warping in the I-profile and the welded connection in support of a cantilever beam, respectively:

$$\sigma_\omega = \left| \frac{B_o \cdot \omega_1}{I_\omega} \right| \tag{4}$$

$$\sigma_{\omega š} = \frac{\sigma_{\omega 1} \cdot t}{2 \cdot a_š} \tag{5}$$

The quantities present in (4) and (5) are determined according to [21], where:

$$B_o = -E \cdot I_\omega \cdot C_o \cdot C_\omega \tag{6}$$

$$I_\omega = \frac{1}{24} \cdot t \cdot h_1^2 \cdot b^3 \tag{7}$$

$$C_o = \frac{M_{\omega t} \cdot \alpha}{G \cdot I_t} \tag{8}$$

$$\alpha = \sqrt{\frac{G \cdot I_t}{E \cdot I_\omega}} \tag{9}$$

$$G = \frac{E}{2 \cdot (1+\nu)} \tag{10}$$

$$I_t = \frac{1}{3} \cdot \left(2 \cdot b \cdot t^3 + h \cdot d^3\right) \tag{11}$$

$$C_\omega = tgh\left(\alpha \cdot L\right) - \frac{B_s \cdot \alpha}{M_{\omega t} \cdot \cosh\left(\alpha \cdot L\right)} \tag{12}$$

$$B_s = F_z \cdot \omega_1 - \frac{M_{y1} \cdot h_1}{2} \tag{13}$$

$$\omega_1 = -\frac{1}{4} \cdot b \cdot h_1 \tag{14}$$

where B_o and B_s are bi-moments, $M_{\omega t} = M_z$ is the torsion moment, I_ω is the sectorial moment of inertia, I_t is the torsional moment of inertia, α is the torsion parameter, G is the shear modulus of the plate, E is the elastic modulus of the plate, ν is Poisson's ratio of the plate, ω_1 is the sectorial coordinate at point 1, and C_o and C_ω are constants, [21].

The maximum stresses due to bending moments and tensile force in the I-profile and the welded connection in support of a cantilever beam, respectively:

$$\sigma_z = \frac{M_x}{W_x} - \frac{M_y}{W_y} + \frac{F_z}{A_p} \tag{15}$$

$$\sigma_{z\check{s}} = \frac{M_x}{W_{x\check{s}}} - \frac{M_y}{W_{y\check{s}}} + \frac{F_z}{A_{\check{s}}} \tag{16}$$

where W_x and W_y are section moduli for the I-profile, $W_{x\check{s}}$ and $W_{y\check{s}}$ are section moduli for the welded connection in support of a cantilever beam (Figure 2), and M_x and M_y are bending moments in x and y direction (Figure 1), respectively:

$$M_x = \frac{F_z \cdot h_1}{2} \tag{17}$$

$$M_y = M_{y1} - \frac{F_z \cdot b}{2} \tag{18}$$

The total stresses in the I-profile (σ_u) and the welded connection in support of a cantilever beam ($n_{\check{s}}$), respectively:

$$\sigma_u = \sigma_\omega + \sigma_z \leq \sigma_d \tag{19}$$

$$n_{\check{s}} = \sigma_{\omega\check{s}} + \sigma_{z\check{s}} \leq \sigma_{\check{s},d} \tag{20}$$

The permissible stresses in the I-profile (σ_d) and the welded connection in support of a cantilever beam ($\sigma_{\check{s},d}$), respectively:

$$\sigma_d = \frac{R_e}{\nu_1} \tag{21}$$

$$\sigma_{\check{s},d} = 0.75 \cdot \beta \cdot \sigma_d \tag{22}$$

where $\beta = 1$, for $a_{\check{s}} \leq 7\ mm$; $\beta = f(a_{\check{s}})$, according to [21], for $a_{\check{s}} > 7\ mm$.

The constraint functions are defined based on previously determined stresses in the material of the I-section and the welds in the beam support and limitation imposed by welding technology [21]:

$$g_1 = \sigma_u - \sigma_d \leq 0 \tag{23}$$

$$g_2 = n_š - \sigma_{š,d} \leq 0 \tag{24}$$

$$g_3 = a_š - 0.7 \cdot \min(t,d) \leq 0 \tag{25}$$

2.3. Metaheuristic Algorithms

The optimization of the considered example was carried out by applying seven selected metaheuristic optimization algorithms. The following algorithms were applied: Moth-Flame Optimization (MFO) algorithm, Multi-Verse Optimizer (MVO), Ant Lion Optimizer (ALO), Whale Optimization Algorithm (WOA), Sine Cosine Algorithm (SCA), Dragonfly Algorithm (DA), and Locust Search (LS) algorithm, [4-6, 9, 14, 15, 22].

The Moth-Flame Optimization (MFO) algorithm is a population-based nature-inspired algorithm, based on the computer simulation of the navigation of moths, [4]. The Multi-Verse Optimizer (MVO) is a nature-inspired algorithm, based on three concepts in cosmology: white hole, black hole, and wormhole, [5]. The Ant Lion Optimizer (ALO) is an algorithm that mimics the hunting mechanism of antlions in nature, [6]. Similar to the previous, Whale Optimization Algorithm (WOA) mimics the social behaviour of humpback whales. This algorithm is inspired by the bubble-net hunting strategy, [9]. The Sine Cosine Algorithm (SCA) is a population-based algorithm that creates multiple initial random candidate solutions and requires them to fluctuate outwards or towards the best solution using the sine and cosine functions, [14]. The Dragonfly Algorithm (DA) is a swarm intelligence optimization method, inspired by the static and dynamic swarming behaviours of dragonflies in nature, [15]. The Locust Search (LS) algorithm is a nature-inspired algorithm, based on the behaviour of swarms of locusts, [22].

2.4. Results of Optimization

The application of the selected optimization algorithms was carried out on the considered example of a cantilever beam, where the following optimization parameters were adopted for all algorithms:

N = 100 - the population size; *Number of iteration* = 1000 - the maximum number of iterations.

The objective function are defined by (3). Constrained functions are defined by (23)-(25).

The bound values of variables are:

$$20 \leq x_1 \leq 30,\ 20 \leq x_2 \leq 80,\ 0.6 \leq x_3 \leq 4,\ 0.5 \leq x_4 \leq 3,\ a_{š,\min} \leq x_5 \leq 1.2.$$

The minimum weld thickness, accordin to [21], is: $a_{š,min} = 3\ mm$.

The input parameters for the optimization process are (Figure 1):

$$L = 200\,cm,\ M_z = 300\,kNcm,\ M_{y1} = 350\,kNcm,\ F_z = 250\,kN,\ E = 21000\frac{kN}{cm^2},\ R_e = 35.5\frac{kN}{cm^2},\ \nu = 0.3,\ \nu_1 = 1.5,$$

where L is the length of a cantilever beam, M_z, M_{y1}, and F_z are loads that act on a cantilever beam, R_e is the minimum value for the yield stress, and v_1 - is load case 1 factored load coefficient.

All algorithms were run several times, and the results from two simulations were chosen and given in the following tables and convergence diagrams (Table 1 and Table 2, Figure 3 and Figure 3).

Tables 1 and 2 show the optimization results for all seven metaheuristic algorithms applied to the considered example. Besides obtained optimized section areas (Best – the best value) and optimized variable values, each algorithm's characteristics are shown (Worst – the worst value, Mean – the mean value, Std – standard deviation, and Time - optimization run time).

There was no violation of the constraint functions in all applied algorithms within the optimization process execution (values g_1, g_2 and g_3, Table 1 and Table 2).

Table 1: Optimization results for Simulation 1

	MFO	ALO	DA	LS	WOA	SCA	MVO
Best [cm²]	133.948	134.994	137.143	134.537	137.910	137.370	134.625
Worst [cm²]	214.979	203.246	234.435	243.024	296.139	203.452	231.039

	MFO	ALO	DA	LS	WOA	SCA	MVO
Mean [cm^2]	134.578	135.649	138.267	135.661	141.898	139.439	137.850
Std	5.759	3.086	6.838	5.590	10.164	4.671	6.754
Time [s]	2.885	37.075	73.481	80.728	3.907	2.916	4.831
g_1	-2.5221	-2.9998	-3.0209	-3.2411	-3.8660	-3.3827	-3.3591
g_2	0	0	-0.3650	0	0	-0.2626	0
g_3	0	0	0	0	-0.0411	-0.0007	0
x_1 [cm]	29.0681	24.6512	30.0	22.7058	23.1879	25.0776	21.8516
x_2 [cm]	20.0	20.0	20.0	20.0	20.0	20.0	20.0
x_3 [cm]	1.7143	1.7143	1.7143	1.7147	1.7462	1.7152	1.7145
x_4 [cm]	1.7143	2.5237	1.7143	2.8334	2.8463	2.5671	2.9849
x_5 [cm]	1.2	1.2	1.2	1.2	1.1813	1.2	1.2

Table 2: Optimization results for Simulation 2

	MFO	ALO	DA	LS	WOA	SCA	MVO
Best [cm^2]	134.507	133.985	133.948	134.090	140.066	139.031	133.994
Worst [cm^2]	194.027	247.817	190.042	169.281	284.358	209.991	248.398
Mean [cm^2]	134.852	134.585	135.015	140.531	142.209	142.783	135.595
Std	3.160	4.219	5.046	5.644	7.273	5.628	5.185
Time [s]	4.044	46.826	115.944	100.556	4.918	4.096	5.415
g_1	-3.2558	-2.5248	-2.5222	-2.5397	-3.2804	-3.5510	-2.5206
g_2	0	0	0	-0.0102	0	-0.0679	0
g_3	0	0	0	0	-0.0374	-0.0334	0
x_1 [cm]	22.551	29.0474	29.0677	29.0657	29.1140	26.0471	29.1205
x_2 [cm]	20.0	20.0	20.0	20.0	20.0	20.0	20.0
x_3 [cm]	1.7143	1.7143	1.7143	1.7143	1.6965	1.7272	1.7126
x_4 [cm]	2.8595	1.7197	1.7144	1.7215	2.0641	2.4527	1.7126
x_5 [cm]	1.2	1.2	1.2	1.2	1.1502	1.1757	1.1988

For some algorithms, 100 iterations are enough to achieve an optimum solution (convergence diagrams in Figure 3 and Figure 4), while some algorithms need 500 or 1000 iterations, which means that the chosen number of iterations was chosen adequately to make the comparison in this case.

It is noticeable that the optimum value of variable $x_2 = h$ is its minimum (Table 1 and Table 2). On the opposite, the optimized value of variable $x_5 = a_s$ is at its upper bound (maximum) or close to it.

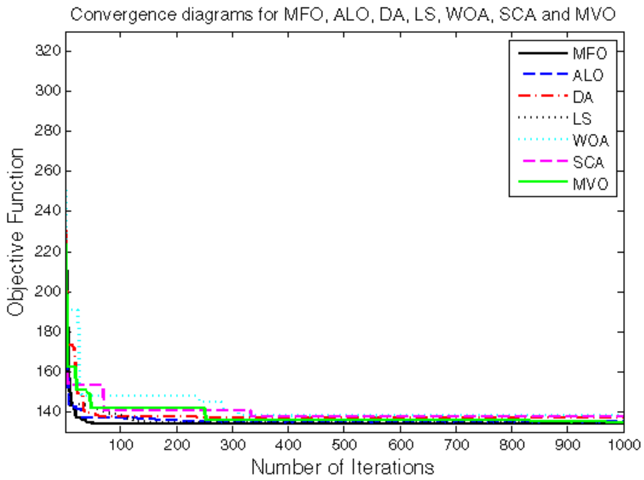

Figure 3: Convergence diagrams for Simulation 1

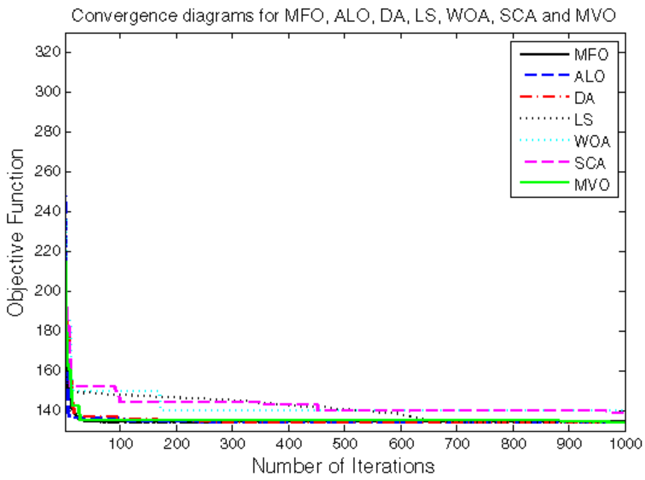

Figure 4: Convergence diagrams for Simulation 2

3. CONCLUSION

This research presents the importance of applying metaheuristic optimization algorithms to mechanical and structural design problems. Also, seven algorithms are applied to a single-objective engineering problem. The objective function is the cross-sectional area of the welded I-profile, shown in Figure 2. The optimization problem has five variables and three constraint functions. The results are taken out of two simulations per each applied algorithm.

For the considered case, input data and optimization parameters, it has been revealed that MFO reaches the optimum value for the shortest time (Table 1 and Table 2). Also, WOA, SCA, and MVO reach the optimum value quickly. However, all other algorithms need significantly longer to optimize, especially DA and LS algorithms.

By looking at the obtained optimum values and differences in constraint functions (g_1, g_2 and g_3), the tables show that WOA and SCA algorithms yield the poorest results compared to other algorithms (Table 1 and Table 2, Figure 3 and Figure 4). Moreover, the WOA algorithm has the greatest standard deviation (Table 1 and Table 2).

MFO and MVO algorithms emerged as the most appropriate considering the minimum cross-sectional area values, standard deviation, and optimization time. However, the MFO algorithm might be modified to mitigate early convergence (Figure 3 and Figure 4), which would improve the accuracy. The ALO algorithm is also very suitable for the application in terms of accuracy and standard deviation but should be improved to shorten the processing time.

Further research needs new algorithms to be tested on specific engineering problems with many variables and constraint functions, both in single-objective and multi-objective optimization problems. Finally, the researchers should undertake modifications, hybridizations and improvements of algorithms and their parameters to improve accuracy, convergence and speed.

ACKNOWLEDGEMENTS

This work has been supported by the Ministry of Education, Science and Technological Development of the Republic of Serbia, through the Contracts for the scientific research activity realisation and financing in 2022, 451-03-68/2022-14/200108 and 451-03-68/2022-14/200102.

REFERENCES

[1] Q. Qi, Y. Yu, Q. Dong, G. Xu and Y. Xin, "Lightweight and green design of general bridge crane structure based on multi- specular reflection algorithm", Advances in Mechanical Engineering, Vol. 13(10), pp. 1–15, (2021), https://doi.org/10.1177/16878140211051220

[2] M. Savković, R. Bulatović, M. Gašić, G. Pavlović and A. Stepanović, "Optimization of the box section of the main girder of the single-girder bridge crane by applying biologically inspired algorithms", Engineering Structures, Vol. 148, pp. 452-465, (2017), https://doi.org/10.1016/j.engstruct.2017.07.004

[3] G. Pavlović, M. Savković, N. Zdravković and G. Marković, "Comparative analysis and optimization of T and I cross sections of crane hook using by two physics-inspired algorithms," IMK-14 - Istraživanje i razvoj, Vol. 25(3), pp. 87-94, (2019), DOI: 10.5937/IMK1903087P

[4] S. Mirjalili, "Moth-flame optimization algorithm: A novel nature-inspired heuristic paradigm", Knowledge-Based Systems, Vol. 89, pp. 228-249, (2015), https://doi.org/10.1016/j.knosys.2015.07.006

[5] S. Mirjalili, S.M. Mirjalili and A. Hatamlou, "Multi-Verse Optimizer: a nature-inspired algorithm for global optimization", Neural Comput & Applic, Vol.27, pp. 495–513, (2016), https://doi.org/10.1007/s00521-015-1870-7

[6] S. Mirjalili, "The Ant Lion Optimizer", Advances in Engineering Software, Vol.83, pp. 80–98, (2015), https://doi.org/10.1016/j.advengsoft.2015.01.010

[7] S. Arora and S. Singh, "Butterfly optimization algorithm: a novel approach for global optimization", Soft Comput, Vol. 23, pp. 715–734, (2019), https://doi.org/10.1007/s00500-018-3102-4

[8] S. Arora, S. Singh and K. Yetilmezsoy, "A modified butterfly optimization algorithm for mechanical design optimization problems", J Braz. Soc. Mech. Sci. Eng., Vol. 40, Article ID 21, p. 17, (2018), https://doi.org/10.1007/s40430-017-0927-1

[9] S. Mirjalili and A. Lewis, "The Whale Optimization Algorithm", Advances in Engineering Software, Vol. 95, pp. 51–67, (2016), https://doi.org/10.1016/j.advengsoft.2016.01.008

[10] S. Mirjalili, A.H. Gandomi, S.Z. Mirjalili, S. Saremi, H. Faris and S.M. Mirjalili, "Salp Swarm Algorithm: A bio-inspired optimizer for engineering design problems", Advances in Engineering Software, Vol. 114, pp. 163-191, (2017), https://doi.org/10.1016/j.advengsoft.2017.07.002

[11] G. Dhiman and V. Kumar, "Emperor penguin optimizer: A bio-inspired algorithm for engineering", Knowledge-Based Systems, Vol. 159, pp. 20–50, (2018), https://doi.org/10.1016/j.knosys.2018.06.001

[12] G. Dhiman and A. Kaur, "STOA: A bio-inspired based optimization algorithm for industrial engineering problems", Engineering Applications of Artificial Intelligence, Vol. 82, pp. 148–174, (2019), https://doi.org/10.1016/j.engappai.2019.03.021

[13] A.S. Heidari, R.A. Abbaspour and A.R. Jordehi, "An efficient chaotic water cycle algorithm for optimization tasks", Neural Comput & Applic, Vol. 28, pp. 57–85, (2017), https://doi.org/10.1007/s00521-015-2037-2

[14] S. Mirjalili, "SCA: A Sine Cosine Algorithm for solving optimization problems", Knowledge-Based Systems, Vol. 96, pp. 120-133, (2015), https://doi.org/10.1016/j.knosys.2015.12.022

[15] S. Mirjalili, "Dragonfly algorithm: a new meta-heuristic optimization technique for solving single-objective, discrete, and multi-objective problems", Neural Comput & Applic, Vol.27, pp. 1053–1073, (2016), https://doi.org/10.1007/s00521-015-1920-1

[16] A. Kaveh and A. Zolghadr, "Cyclical Parthenogenesis Algorithm: A New Metaheuristic Algorithm", Asian Journal of Civil Engineering (BHRC), Vol. 18(5), pp. 673-701, (2017)

[17] A. Kaveh, S.R.H. Vaez and P. Hosseini, "Matlab Code for an Enhanced Vibrating Particles System Algorithm", Int. J. Optim. Civil Eng., Vol. 8(3), pp.401-414, (2018)

[18] A. Kaveh and A.D. Eslamlou, "Metaheuristic Optimization Algorithms in Civil Engineering: New Applications", Springer Nature Switzerland AG, Cham (Switzerland), (2020), https://doi.org/10.1007/978-3-030-45473-9

[19] O. Skoglund, J. Leander and R. Karoumi, "Optimizing the steel girders in a high strength steel composite bridge", Engineering Structures, Vol. 221, Article ID 110981, p. 10, (2020), https://doi.org/10.1016/j.engstruct.2020.110981

[20] H. Abedini, S.R.H. Vaez, and A. Zarrineghbal, "Optimum design of buckling-restrained braced frames", Structures, Vol. 25, pp. 99–112, (2020), https://doi.org/10.1016/j.istruc.2020.03.004

[21] Z. Petković and D. Ostrić, "Metalne konstrukcije u masinogradnji I", University of Belgrade, Faculty of Mechanical Engineering, Belgrade (Serbia), (1996)

[22] E. Cuevas, A. González, F. Fausto, D. Zaldívar and M. Pérez-Cisneros, "Multithreshold Segmentation by Using an Algorithm Based on the Behavior of Locust Swarms", Mathematical Problems in Engineering, Vol. 2015, Article ID 805357, p. 25, (2015), https://doi.org/10.1155/2015/805357

ORIGINAL SCIENTIFIC PAPER OPEN ACCESS

Sensitivity of a Simple Earthquake Nucleation Model to Small Parameter Perturbation: Conditions for the Occurrence of Deterministic Chaos

Srđan Kostić[1*], Nebojša Vasović[2], Jelena Trivan[3]

[1] Jaroslav Černi Water Institute, Belgrade, Serbia

[2] University of Belgrade, Faculty of Mining and Geology, Belgrade, Serbia

[3] University of Banja Luka, Faculty of Mining Prijedor, Prijedor, Bosnia and Herzegovina

ARTICLE INFO

* **Correspondence:** srdjan.kostic@jcerni.rs

DOI: 10.5937/engtoday2201027K

UDC: 621(497.11) **ISSN:** 2812-9474

Article history: Received 9 February 2022; Accepted 3 March 2022

ABSTRACT

A new mechanism that may account for the onset of chaotic dynamics of earthquake faults is proposed and analyzed. The concept is to build on the Burridge-Knopoff model, which integrates the spring-block setup with the Dieterich-Ruina's rate- and state-dependent friction law to interpolate for the key aspects of earthquake episodes, including the seismic nucleation, fracture propagation and arrest, as well as the rupture healing. Results obtained indicate that determistic chaos occur in case frictional parameters exhibit small oscillations about their equilibrium values. Based on the construction of appropriate phase portraits, power spectra and the Lyapunov exponents it could be concluded that a single time-dependent parameter is sufficient for the chaotic behavior to emerge, while the fully developed chaos is found when two perturbed parameters are brought into play.

KEYWORDS

Spring-block model, External perturbation, Deterministics chaos

1. INTRODUCTION

The issues of seismogenesis, fracture propagation and healing, as well as the complex spatial, temporal and magnitude correlations linked to the observed earthquake patterns lie in the focus of an interdisciplinary research. Its advances are not important only for the scientific part on understanding the driven dissipative systems, but can also prove beneficial for their possible practical ramifications. A widely accepted definition states that earthquakes constitute stick-slip frictional instabilities recurring on preexisting faults driven by the slowly moving tectonic plates. In particular, each earthquake episode comprises a long-term phase of stress accumulation and a sudden jerky displacement accompanied by stress relaxation. Though there is no comprehensive framework that may account for all the related complex phenomena, it has come to light that the frictional laws, entering the earthquake models as "force" terms, are likely to be the crucial factor governing the statistical properties of earthquakes. Consistent with this, the physics of seismic phenomena is concerned both with the friction and fracture features relevant to the description on the microscopic level, and the application of statistical methods providing for the general event distributions on the macroscopic level. In terms of the former, the underlying friction laws can become complicated to say the least, involving not only the velocity and displacement dependencies, but also being contingent on the previous history ("prestress" from earlier cycles) and the "state" of the contact surface (interfacial layer). As for the event distributions, the long-term patterns of seismic activity can broadly be cast in two categories, one referring to periodic or quasiperiodic sequences of "characteristic" earthquakes (mainshocks) similar in spatial extent and moment, while the other encompasses the aperiodic activity patterns, where a wide range of event sizes can be expected. The rationale for the events obeying some systematic behavior often comes down to two scenarios: either there is a multicomponent fault with persistent segmentation, or the interaction of several faults may take place, such that the influence of all but one (master fault) can be neglected. Regarding the aperiodic behavior, the possible scenarios are more diverse. If the faults are made up of multiple segments which are only partially locked, the transfer of stress and its interplay with prestress may lead to local events where a single segment or a cluster of segments can take part, as well as the major events that break out along the entire seismogenic zone. The more likely setup for aperiodic behavior involves spatial variations (heterogeneity) of the friction laws, as patches of materials with different frictional properties may be embedded within an otherwise homogeneous fault. However, for the analysis pursued in the current paper, it is of greater importance that the aperiodic sequences of events can be linked to quite different dynamical backgrounds. Primarily, one may have low-dimensional data sets that are best accounted for by the deterministic chaos, or there may be some high-dimensional data sets, whose generation can naturally be attributed to stochastic (random) processes. One should caution for the instances where it may be difficult to distinguish between the stochastically perturbed deterministic chaos and the genuine random processes. Apart from the above opposition, a comparably novel explanation suggested for the aperiodic behavior, in particular the power-law magnitude-frequency distribution determined by the Gutenberg-Richter law, relies on the concept of self-organized criticality, by which the fault is assumed to consistently operate on a brink of a failure, such that the slow loading enables the system to self-organize into a dynamical critical state which lacks any characteristic time or length scale.

The paper is organized as follows. In section 2, we provide some background on the considered models, discussing the phenomena related to the original system and the introduced modifications. In section 3 we formally introduce the extended model, assuming that one or two system parameters are periodically perturbed. The section proceeds with the detailed local bifurcation analysis, supported by the phase portraits, power spectra and the calculation of the maximal Lyapunov exponent, the latter offering evidence for the chaotic behavior in the extended model. In section 4 we attempt to provide a seismological interpretation of the obtained results. Concluding remarks are given in section 5, where a brief summary of the results is followed by the discussion on possible implications to the earthquake phenomena, outlining the issues for further research.

2. BACKGROUND ON THE ORIGINAL MODEL AND ITS DERIVATIVES

In the present paper, we build on the Burridge-Knopoff (BK) model [1], which is counted among the canonical models of the fault dynamics. In the simplest configuration, it comprises a single block which is connected to the rigid loader plate via a stiff spring and lies on the frictional sliding surface analogous to the fault, see Fig. 1. The dynamics described by the usual one-dimensional version is likely to fit best the motion of large earthquakes that span the depth of the schizosphere and tend to propagate only in one dimension along the fault. The basic model and its various derivatives have proven capable of capturing the nucleation process accompanied by the low magnitude aseismic slips localized to the compact "seed" area of the rupture, kinematics of the rupture spreading and the dynamics of the fracture healing process. Nonetheless, in recent years the BK model has attracted much attention for efficiently reproducing the statistical properties of sequences of recurring earthquake events [2-5]. For this line of research, one of the key factors turns out to be the accurate representation of the involved characteristic spatial and temporal scales. In terms of the dynamics displayed, the focus in the BK model lies with the interplay of the driving and the friction forces which generates the stick-slip type of motion, paradigmatic for the propagation of earthquakes. In particular, the earthquake itself corresponds to the ''slip'' phase, whereas the ''stick" stage reflects the interseismic period of the elastic strain accumulation. For the onset of a slip, the force acting on a block has to overcome the static friction with the surface. Nonetheless, in order for the model to exhibit a dynamical instability which allows for the fracture propagation, it is essential that the friction force possesses a frictional weakening property, meaning that the friction should become weaker as the block slides.

The formulation of a plausible friction law requires a deeper insight into the physics of an interfacial layer between the block and the rough surface, given that the interface bears the local pressures approaching the material yield strength, which renders its properties substantially different from those of the surrounding elastic medium. From the microscopic point of view, the key ingredient to friction is the notion of asperity micro-contacts, these being the discrete local junctions between the protrusions from the two surfaces brought into contact. The ensemble of asperities defines the genuine total area of contact which is much smaller than the nominal geometrical one. The onset and cessation of a slip are closely tied to the dynamics of the population of the asperities: the latter are rapidly detached just before the slip initiation, whereas the slip arrest promotes their renewal and strengthening. The slip itself is found to consist of two distinct phases, sharply distinguished by the characteristic time of duration and the slip rate. The initial, rapid slip phase, which commences immediately after the breaking of the asperities, is associated with an order of magnitude larger slip velocity than the proceeding slow slip phase.

These types of data, collected from a large number of experiments conducted under laboratory conditions within the velocity-step, slide-hold-slide and similar setups, have led to several constitutive friction laws, which have been successfully applied to explain for the various aspects of the stable and unstable sliding between the elastic solids. Such laws include the dependence of the friction strength on the slip velocity, as well as on a single or multiple evolving state variables which characterize the dynamics of the asperity contacts. In the present paper, we use the Dieterich-Ruina rate-and-state dependent friction law [1] which reads:

$$\mu = \mu 0 + A\ln\left(\frac{\nu}{\nu 0}\right) + B\ln\left(\frac{\nu 0\theta}{L}\right)$$
$$\dot{\theta} = 1 - \frac{\nu\theta}{L} \qquad (1)$$

where μ is the friction coefficient and μ_0 presents its value at some reference sliding velocity v_0 . As for the parameters involved, A and B characterize the properties of the material, while L is a characteristic slip distance comparable to a typical asperity length. Finally, v refers to the slip velocity, whereas θ denotes the time-dependent state variable. Regarding the second equation, there are two points to be noted: first, θ has the dimension of time and second, it increases even if $v = 0$.

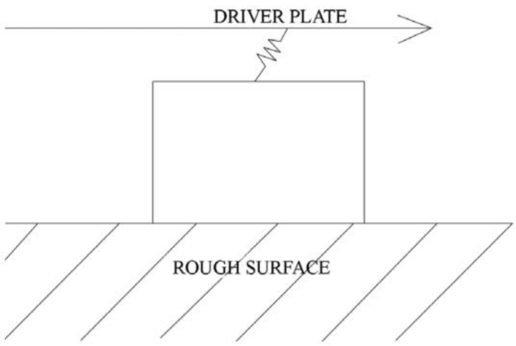

Figure 1: The Burridge-Knopoff model, represented by a slider-block coupled via a stiff spring to the loader plate.

Modification presented in this paper addresses the issue of the system's response to an external perturbation, this aimed at showing that even the small-amplitude influences are sufficient to profoundly change the original behavior, leading to the onset of chaos. Within this framework, the external perturbations are incorporated implicitly by assuming that they induce small oscillations about the equilibrium values of some of the system parameters. Such persistent time-dependent perturbations may be attributed to the Earth tides or the reservoir effects . However, note that the persistence of perturbations should be assessed in relative terms, meaning that even the impact of transient influences whose oscillation period is much shorter than the time they act on the system may still qualify for the provided description. In this context, one recalls the dynamical triggering models, which concern the possibility of earthquakes caused by the passage of seismic waves from the mainshock on some distant fault. In particular, it has been proposed that the stress pulse emitted by the mainshock may increase another fault's slip speed or enhance triggering by reducing the associated state variable.

One should note that analysis of the sensitivity of dynamical system to external perturbations is not limited to earthquake nucleation models, but also is the frequent research topic in other scientific areas [6].

Our numerical simulations of a spring-block model are based on the system of equations coupled with the Dieterich-Ruina rate- and state-dependent friction law are given by

$$\dot{\theta} = -\left(\frac{\nu}{L}\right)\left(\theta + B\log\left(\frac{\nu}{\nu_0}\right)\right)$$
$$\dot{u} = \nu - \nu_0 \qquad (2)$$
$$\dot{\nu} = \left(-\frac{1}{M}\right)\left(ku + \theta + A\log\left(\frac{\nu}{\nu_0}\right)\right)$$

where parameter M is the mass of the block, v_0 stands for the reference (normalizing) velocity, and the spring stiffness k accounts for the linear elastic properties of the bulk medium. Parameter L corresponds to the characteristic friction length, and can be interpreted as the sliding distance for the complete renewal of the population of asperity contacts. The parameters A and B are empirical constants, which depend on the properties of the materials involved. In particular, the parameter A measures the direct velocity dependence ("direct effect"), while $A–B$ is a measure of the steady-state velocity dependence. Note that the friction-related term is the only source of nonlinearity in the model.

For the improved insight into the arising phenomena, we adhere to a common practice of converting the initial system, such as (2), into the non-dimensional one. This is achieved by introducing the scaled variables θ', v', u' and t' defined as: $\theta=A\theta'$, $v=v_0v'$, $u=Lu'$, $t=(L/v_0)t'$. Substituting for the original set of variables θ, v, u and t, the system can finally be recast in the form:

$$\begin{aligned} \dot{\theta} &= -v(\theta+(1+\alpha)log(v)) \\ \dot{u} &= v-1 \\ \dot{v} &= -\eta^2\left[u+\left(\frac{1}{\beta}\right)(\theta+log(v))\right] \end{aligned} \tag{3}$$

where $\alpha=(B–A)/A$ measures the sensitivity of the velocity relaxation, $\beta=(kL)/A$ is the nondimensional spring constant, and $\eta=(k/M)^{1/2}(L/v_0)$ is the nondimensional characteristic frequency.

3. RESULTS

The original model (3) can be modified by assuming the time dependence of the parameters α and β in the following way:

$$\begin{aligned} \dot{\theta} &= -v\left[\vartheta+(1+\alpha(t))log\ v\right] \\ \dot{u} &= v-1 \\ \dot{v} &= -\gamma\eta^2\left[u+\left(\frac{1}{\beta}\right)\left(\theta+log\ v\right)\right] \end{aligned} \tag{4}$$

where $\alpha(t)$, $\beta(t)$ are the positive periodic functions of time:

$$\begin{aligned} \alpha(t) &= \alpha+\delta_\alpha sin(\omega_\alpha t) \\ \beta(t) &= \beta+\delta_\beta sin(\omega_\beta t) \end{aligned} \tag{5}$$

where δ_α, δ_β, ω_α, and ω_β present the constant oscillation amlitudes and the angular frequencies ($\delta_\alpha \leq \alpha$, $\delta_\beta \leq \beta$). Let us proceed with the bifurcation analysis of the model (4) if one or two of the underlying parameters are perturbed, while the remaining ones are held fixed at values admitting the fixed point (Fig. 2).

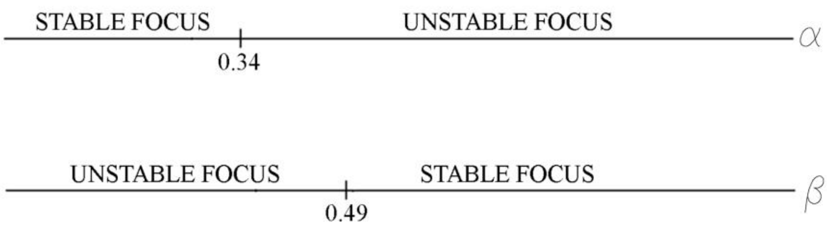

Figure 2: Bifurcations of the system (3) (or (4) if δi=0 is set) under variation of one of the parameters α, β and η. At each instance, the parameters held constant are awarded values that admit the fixed point, α= 0.34, β= 0.49 and η = 0.80

Furhter we exmaine the scenario if only a single parameter, α or β, undergoes small oscillations, while the other parameter is fixed. It turns out that one may observe chaotic behavior irrespective of which of the parameters is perturbed. The typical phase portraits and the power spectra for the corresponding time series are displayed in Fig. 3 (a-b). The emergence of chaotic behavior in these two instances is supported by calculating the maximal Lyapunov exponent, see Fig. 4, which indicates convergence to values above zero.

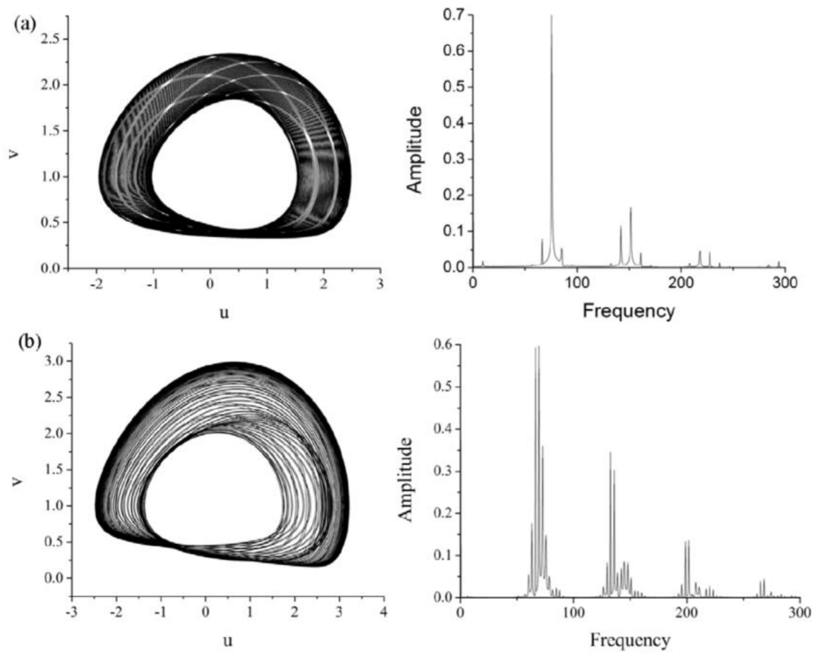

Figure 3: The left column shows the projections on the *(u,v)* plane of the typical orbits of the system (4), whereas the right column displays the corresponding power spectra obtained for the *v(t)* time series. Each row illustrates the system's behavior when the different parameter is periodically perturbed. The perturbation amplitudes are set to: (a) δ_α=0.4, ω_α=0.42 (b) δ_β=0.5, ω_β=0.42 while the equilibrium values of the parameters admit the limit cycle (α=0.4; β=0.5; η=0.8)

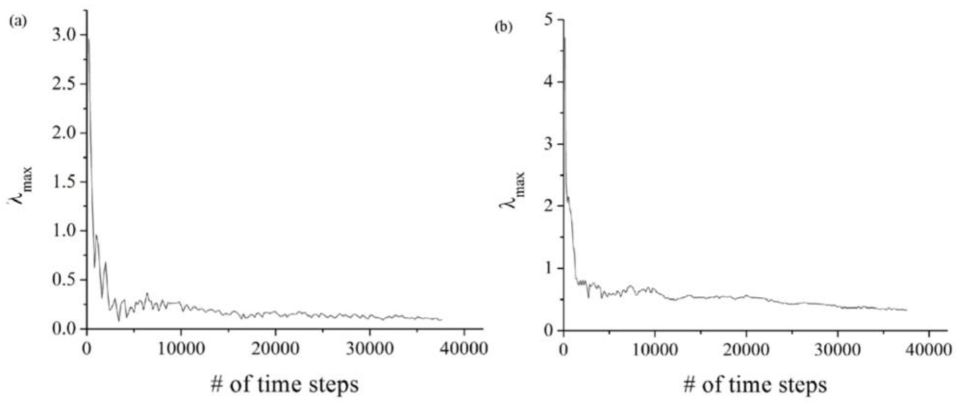

Figure 4: Calculation of the maximal Lyapunov exponent for simulated time series of the block's velocity for δ_α=0.4 in (a) and δ_β=0.5 in (b), respectively. The parameter values correspond to the plots displayed in Figures 4(a) and 4(b). It is demonstrated that the maximal Lyapunov exponents converge well to λ=0.095 in (a) and λ=0.336 in (b).

Further we proceed by examining what occurs if both α and β exhibit small oscillations. For such a scenario, it turns out that the fully developed chaos can indeed emerge, with an instance of the typical phase portrait shown in Fig. 5(a). It is interesting that the inference on the onset of chaos holds true even if the equilibrium parameter values are consistent with the fixed point of the unperturbed system. The conclusions on the character of the observed behavior rely on the power spectrum for the time series *v(t)*, provided in Fig. 5(b), and are further corroborated by the positive value of the maximal Lyapunov exponent, as indicated in Fig. 6. Note that the latter value is significantly larger than in the previous two cases where only a single parameter was perturbed.

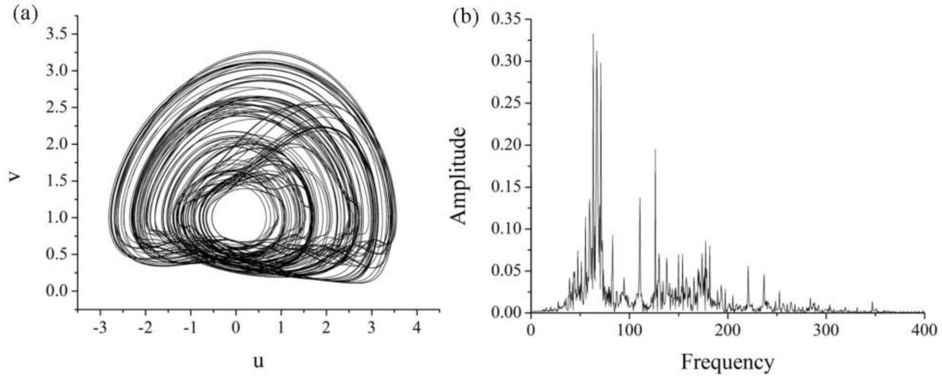

Figure 5: (a) Projection on the *(u,v)* plane of the typical chaotic orbit of the system (4). The results are obtained for the perturbation amplitudes δ_α=0.29 and δ_β=0.4, while the other parameters are set so that the unperturbed system would lie in the fixed point: α=0.29, β=0.5,η=0.8. (b) The power spectrum for the time series *v(t)*.

4. RELATION TO SEISMOLOGY

Though the studied spring-block model provides a greatly simplified picture of the seismic source, it may still shed some light on the mechanics of the fault system. Due to simplifying assumptions, the model is not intended to simulate the behaviour of any real fault, but can highlight the possible mechanisms contributing to the onset of complex behavior observed in the fault dynamics. In these terms, although the parameter values used in this paper are exclusively of theoretical character, without looking for the explicit relation with the observed data concerning the laboratory and natural fault zones, one may attempt to provide a qualitative interpretation of the obtained results. Our analysis involves three main parameters, namely α, β and η. Parameterη, representing the nondimensional characteristic frequency, incorporates the dependence on the parameters with constant values for the observed model: spring stiffness (*k*), mass of the block (*M*), critical slip distance (*L*) and the reference velocity (v_0). This is the reason whyη is held constant during the analysis. On the other hand, parameter α is defined by the ratio of parameters *B-A* and *A*. Parameters *A* and *B* stand for the material properties of the rock, which rely upon the rock type and temperature. These parameters also change during the slip: parameter *A* reflects the rise of the friction coefficient, when the block is subjected to a sudden velocity increase. For every successive slip phase, this parameter gains a new value, accounting for the different nature of the contact between the block and the rough surface. In addition, *A* enters the parameter β, defined as the nondimensional spring constant. Parameter *B-A* is directly connected with the amount of stress released during the ''slip'' phase. In our analysis, we first simulate this dependence by assuming that parameters α and β are periodically time-dependent, without relating to specific rock type and the temperature range. The results obtained indicate that for small perturbations near the fixed point, the system exhibits rich behavior, implying the sensitivity of the observed system on the material properties *A* and *B*. In other words, a transition to chaos is observed by simply changing the value of the parameters *A* and *B*. In an earthquake analogy to the single block, this suggests that the potential transitions to chaos are essentially controlled by the ratio of the parameters *(B–A)* and *A*, as well as the critical length *L* derived from the friction law, but are independent of the elastic feature of the medium surrounding the fault, which is idealized by the parameter *k*.

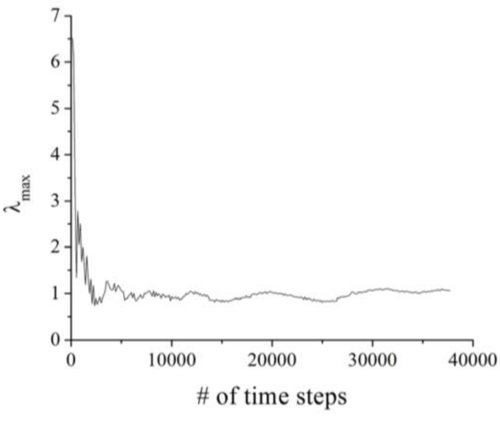

Figure 6: Calculation of the maximal Lyapunov exponent for the simulated time series of the block's velocity at δ_α=0.29 in (a) and δ_β=0.4 in (b), respectively. The other parameter values coincide with those in Fig. 5(a). The maximal Lyapunov exponent is seen to converge well to λ=1.068

5. CONCLUDING REMARKS

In principle, three dynamical paradigms are identified as likely to give rise to aperiodic behavior in the earthquake fault dynamics. These include the deterministic chaos, the stochastic processes and the self-organized citicality, none of which is at the current stage given advantage over the others. What makes the scenario involving deterministic chaos distinct is that it raises the possibility of the system being sensitive to small perturbations in the intrinsic or the external conditions. The purpose of this study has been to suggest the mechanisms that one may build into the minimal model of fault dynamics capable of exhibiting the chaotic behavior. The term „minimal" alludes to the point that even the fault with rather simplistic monoblock structure may still generate complex patterns of seismic activity. The adopted approach lies at variance with most of the models known so far to admit the aperiodic dynamics, given that they commonly invoke multicomponent faults composed of regions which are only partially locked or refer to spatially heterogeneous faults having sections with the different frictional laws intermixed. In particular, we have demonstrated that certain modifications, reflected in introducing the novel, small magnitude variables into the original BK monoblock model, may be sufficient to profoundly influence the system dynamics, eventually leading to the onset of the chaotic regime. In each instance, the observation of chaos is verified by determing the power spectra of the underlying $v(t)$ time series, this corroborated by calculating the corresponding maximal Lyapunov exponent.

The focus of the present paper has been on the effects of external perturbations, which, due to low amplitude, may be incorporated implicitly into the model, having them induce small oscillations of the parameters α and β about their equilibrium values. In case of any single perturbed parameter, while the remaining subset is held fixed, one is unable to find the fully developed chaos. However, we have witnessed the latter once allowing for both α and β to be time-dependent. Note that the fully developed chaos is characterized by the continuous power spectrum of the appropriate time series and the leading Lyapunov exponent significantly above zero.

REFERENCES

[1] S. Kostić, N., Vasović, K., Todorović, L. and Franović, "Nonlinear dynamics behind the seismic cycle: One-dimensional phenomenological modeling," Chaos, Solitons and Fractals, Vol. 106, pp. 310-316, https://doi.org/10.1016/j.chaos.2017.11.037, (2018)

[2] Motchongom, M.T., Kengne, R., Tanekou, G.B., Pelap, F.B., Kofane and T.C., "Complex dynamic of two-block model for earthquake induced by periodic stress disturbances," European Physical Journal Plus Vol.137(2), p.177, https://doi.org/10.1140/epjp/s13360-022-02384-5, (2022)

[3] Nkomom, T.N., Ndzana, F.I., Okaly, J.B. and A. Mvogo, "Dynamics of nonlinear waves in a Burridge and Knopoff model for earthquake with long-range interactions, velocity-dependent and hydrodynamics friction forces," Chaos, Solitons and Fractals, Vol.150, 111196, https://doi.org/10.1016/j.chaos.2021.111196, (2021)

[4] C. Mascia and P. Moschetta, "Numerical evidences of almost convergence of wave speeds for the Burridge–Knopoff model," SN Applied Sciences, Vol. 2(12), 2053, https://doi.org/10.1007/s42452-020-03856-y, (2020)

[5] H. Kawamura, M. Yamamoto and Y. Ueda, "Slow-slip phenomena represented by the one-dimensional burridge–knopoff model of earthquakes," Journal of the Physical Society of Japan, Vol. 87(5), 053001, https://doi.org/10.7566/JPSJ.87.053001, (2018)

[6] V. Shevchenko, "Adaptation of Earth-Moving Machines to External Loading Conditions," IMK-14 – Research & Development in Heavy Machinery 25, EN 7-11, (2019)

ORIGINAL SCIENTIFIC PAPER OPEN ACCESS

Spaces and Technologies of the Circus Spectacle

Marija Divac[1*], Sara Milošević[1], Katarina Jevtić-Novaković[1], Olga Timčenko[2]

[1]Academy of Technical and Art Applied Studies Belgrade/Department School of Civil Engineering and Geodesy of Applied Studies, Belgrade, Serbia

[2] Aalborg University, Department of Architecture, Design and Media Technology, Copenhagen, Denmark

ARTICLE INFO

[*] **Correspondence:** divac.marija90@gmail.com

DOI: 10.5937/engtoday2201035D

UDC: 621(497.11) **ISSN:** 2812-9474

Article history: Received 14 March 2022; Accepted 28 March 2022

ABSTRACT

Contemporary circus is a complex, interdisciplinary form of performing arts. The new circus was built on the basis of the traditional one, but it is more complex than it and brings a combination of elements of acrobatics, dance and drama theater, shadow theater, puppet theater, as well as contemporary visual arts and digital technologies. The circus spectacle, its architectural concept and its content, have changed over the centuries, following social events and the cultural framework of the time. Although the spectacle is still adapting and changing, we ask the question, whether stationary circuses have managed to adapt and transform for the needs of modern society. In this paper, through a brief history of the circus spectacle and important typological characteristics of the objects, one of the most significant objects of this spectacle will be analysed.

KEYWORDS

Circus, Spectacle, Architectural concept, Modern technologies, Transformation.

1. INTRODUCTION

The circus is a space where miracles happen, where seemingly everything is impossible and unreal, and where emotions full of excitement and laughter are awakened. In addition to representing an artistic form of performance, circuses are also representatives of cultural objects. Stationary circuses have been built throughout history, and their future is uncertain. Architecture is often neglected in the numerous literature of the circus spectacle, but the buildings that were built in the past for the needs of this art stand firm today. This type of architecture is now being transformed and adapted to the modern age and new technologies in various ways. The circus facility should have a circular stage, for performing acrobatics, and a grandstand around it, arranged in a circle on all sides to accommodate the audience. This is the main difference in relation to other cultural objects, where the stage spaces are mostly rectangular and located at one end, and not in the central part of the hall. To perform circus disciplines, the space should have width, depth and appropriate height. [1] That is why, throughout history, unique facilities have been built in Europe for this type of artistic spectacle. In this paper, we will present the development trajectory of circus facilities and its transformation.

2. BRIEF HISTORICAL OVERVIEW OF CIRCUS DEVELOPMENT

Circus (lat. circus - circle) belongs to the type of performing arts, because as a rule it serves to present diverse content [2]. We also use the word "circus" for the name of the special facility in which such performances take place. The foundation of circus art is based on the demonstration of the unusual and funny. In the past, the circus was associated with traveling troops, often families who had and were able to show unusual things, but often also deformed people, bizarre skills and, unfortunately, various types of cruelty to animals. Characteristic points of the modern circus include: demonstration of tricks, representation of special abilities, pantomimes, jokes, performances with risk (physical strength, acrobatics, wire walking), as well as acts with trained animals.

The circus building is mostly cylindrical in shape with a high dome and inside there is a stage space with stands for spectators. In circuses, the space of the stage always has the same dimension - 13 m, and it is the same everywhere in the world (given by a request from the 19th century). The explanation for this dimension is the professional minimum for maintaining acrobatics, and acrobatics with horses and other animals are especially emphasized.

The beginnings of the circus date back to before the new era, but the traditional type of circus (as we know it today) appeared only at the end of the 18th century in London, when Philip Astley built a round hall. They began to hold performances that consisted of exercises on horses and some acrobatics. Several other spaces organized in this way were created in a short period of time, but the plays were copied as in Astley's. [3]

In the eighteenth century, only free surfaces were taken, which were gradually closed with grandstands and domes. The reason for that is simpler charging of tickets for the spectacle, but also prevention of natural disasters that affect their maintenance. The circus was something new, but the use of wood as a material was simple and similar to other buildings in this century.

Figure 1: Philip Astley's First Riding Space (Astley's Amphitheater) 1770

By the end of the 19th century, the idea of a circus had spread throughout Europe. The first circus made of solid material was built by Astley, in Paris, where he presented somewhat more diverse performances, but most of them were attractions on horses. Later Astley's inheritors, the Italians Franconi, built a new circus in which they had a more diverse program, with ideas of mimicry and wild animal fights with humans and dogs. [4]

Circus facilities in Russia were initially built of wood during the wars, and the fires themselves mostly killed everyone, but that was no reason for them to be forgotten. New and massive facilities were built in the same places in a short period of time, and over time there were more of them that were built in accordance with the new times and up-to-date technologies. [5]

In the nineteenth century, circus buildings required more attention. The splendor of the time influenced the objects of this purpose to switch to more durable materials and that their exteriors contribute to the beauty of the larger cities in which they were created. As circus performances were more popular on the European continent, the role of architecture was to attract more visitors. The buildings were massive but also more attractive, larger in size and richly decorated.

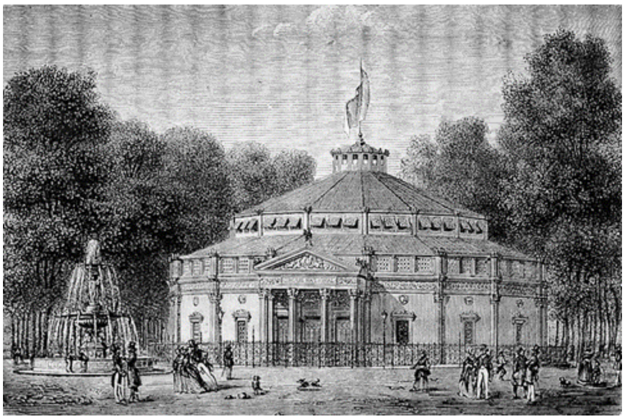

Figure 2: The National Circus des Champs-Elysées (Cirque National des Champs-Elysées) in 1841

In the twentieth century, there are great and sudden changes, caused by wars and political regimes. [6] Stationary circus facilities, after the Second World War, were increasingly built in countries with socialist regimes, and circuses became less popular in capitalist countries. The style of construction has changed. At the beginning of the century, massive circus objects were represented in the western part of Europe. Later, in socialist countries, transparent glass facades with quite complex geometries of roof constructions became popular.

Figure 3: Metropolitan Circus in Bucharest (Circul Metropolitan București) 1960.

In the twenty-first century, there is no construction of new circus facilities. For the circus performance, buildings mostly from the twentieth century are used. The reconstructions are aimed at preserving these giants and creating security due to various extraordinary circumstances.

Diagram 1: Prevalence of circus facilities in Europe in the 21st century

3. TYPOLOGICAL CLASSIFICATION OF CIRCUS ARCHITECTURAL SPACE

The basic elements of a stationary circus determine its classification. What is typical for circus facilities is the main arena (with stage and stands) and auxiliary space where all the accompanying elements are located (wardrobe and all premises for artists, auxiliary stage space, animal cages, etc.). Therefore, it is primarily possible to make a simple division of plans of circus facilities:

- compact solutions, where all parts form one whole, primarily this refers to the ground floor of the building;

- two-part solutions with a clear division into the main stage part and auxiliary accompanying space. [7,8].

3.1. Typological classification according to geometric shapes of objects

Circus buildings are characterized by different geometric shapes. Some projects are typical and thanks to them, several buildings were built on that principle. [9,10] The most common shape of the base is a circle or octagon, and the roof structures of the dome or rectilinear surface, mostly hyperbolic paraboloids and their sections.

3.2. Typological classification of internal organization of space

The circus consists of a stage in the middle and around the stands, and further there are auxiliary rooms, halls and places for storing equipment and animals. The space of the podium can be variable, ie. there can be more platform for performances and the diameter is always 13m. [11,12]

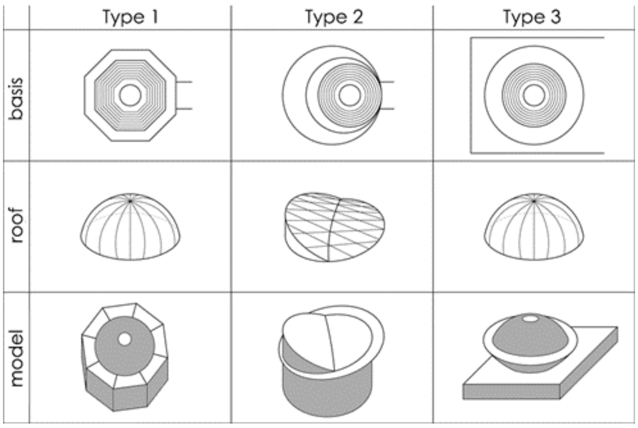

Diagram 2: Typological classification of circus objects represented in the eastern part of Europe

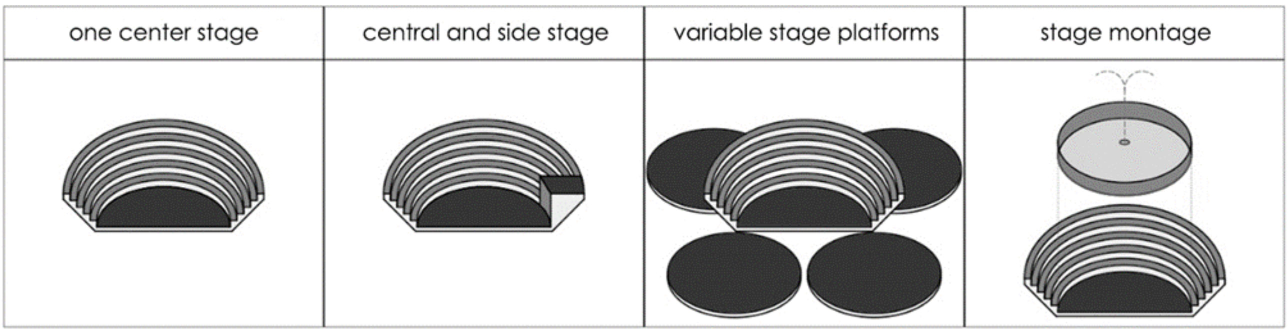

Diagram 3: Typological classification of stage spaces

4. CASE STUDY - GREAT MOSCOW CIRCUS ON VERNADSKY AVENUE

In the 1950s, Moscow became a center of international and domestic tourism, and the city needed new cultural facilities, including a circus. There was already a circus building on Tsvetnoy Boulevard [13] in Moscow, but there was a need for another one. The circus on Vernadsky Avenue was built under the direction of architect Jefim Petrovič Vulih, and was opened in 1971. This circus is considered one of the largest stationary circuses in the world (the third largest).The capacity of the stands is such that it can accommodate 3,400 spectators in 23 rows, and the height of the amphitheater is 36 meters.

The shape of the building consists of a cylindrical base and a roof structure formed by hyperbolic paraboloids. The dome attracts special attention, both during the day with its clown hat appearance and at night in differently lit colors. The space of the main hall, as with most circuses, has the shape of an inverted fringed cone, the lowest part begins with a stage of 13 meters and ends with the largest diameter of 25 meters, ie. with an area of almost 2000m2. [14]

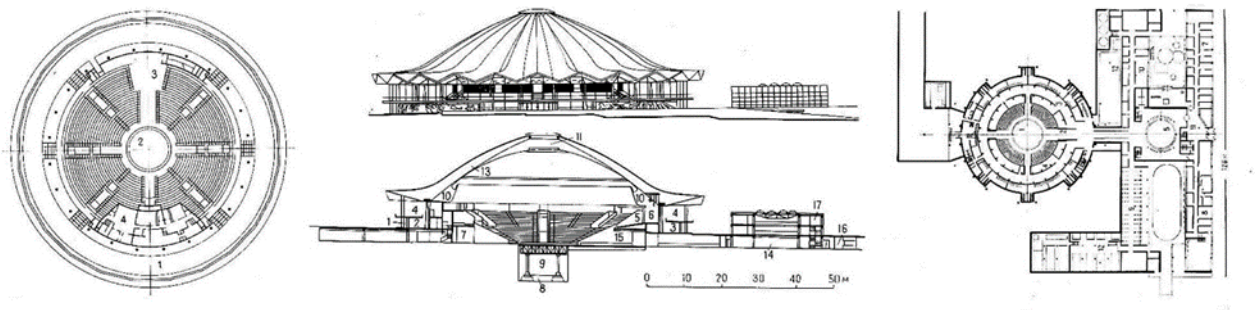

Figure 4: Circus layout

This giant has not had any major changes in its 45 years. As there are a large number of circuses in Russia, the Ministry of Culture manages to renew 2 to 3 circuses a year. For the circus on Vernadsky Avenue, only the emergency elements have been renovated, such as the leaking roof, offices, ballet halls and the space where the animals are kept. Only a few years ago, controversies began about how it is time for a major reconstruction of the entire circus and the area around it.

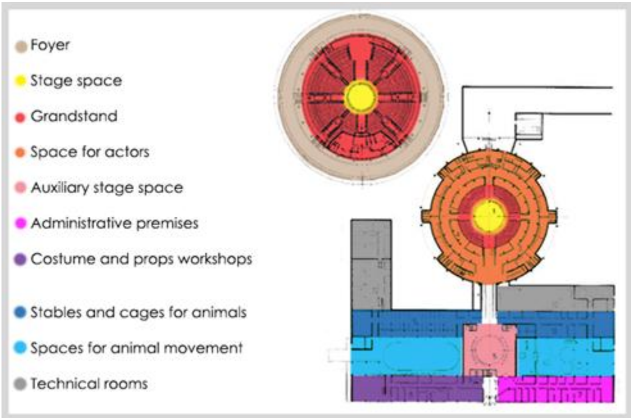

Figure 5: Room representation

Animal spaces, administration and technical rooms are located in the auxiliary building and connected by a warm connection with the stage. The basic division of the space for animals consists of accommodation and exercise rooms, and between them is a training stage of the same dimensions, 13 m in diameter, and this part of building is directly connected to the main stage. However, in the time of the development of technology, the Internet and visual, sound and other effects, he brought the circus into a period of adaptation and improvement. [15,16] For security reasons, about 200 cameras have been set up throughout the circus. A novelty in this circus is the appearance of a screen 34 m long in a circle inside the dome (it extends 360 °). His role is to accompany each performance with a visual representation and to distract attention when changing spectacular acts. It is located above the stands and its height is 3m. There are also independent, smaller screens showing circus events and news during breaks and before the show begins. In this way, the scene managed to modernize and adapt to the current time. One of the interesting facts about the Great Moscow Circus is that there is still room for a live orchestra that still works on that principle, as in the theater, creating music and the necessary effects for some performances.

4.1. Variable stage platform

This unique engineering mechanism was designed by Andrej Vladimirovič Platov and does not exist in any other circus in the world. The idea was to build not only something big, but also unusual. This is how the idea of making the stage space transformable arose, which is achieved by using mobile platforms or "manege", as the Russians call them. The circus is unique in its arena, because it is possible to change five different platforms: ice, light, water, illusion and platform for horses. In the basement of the building there is a space where there are mechanical assemblies, which enable stage changes and allow the variable to take place in a very short time (5 minutes). During the shift, clowns remain on the stage to make the transition look even shorter. [17]

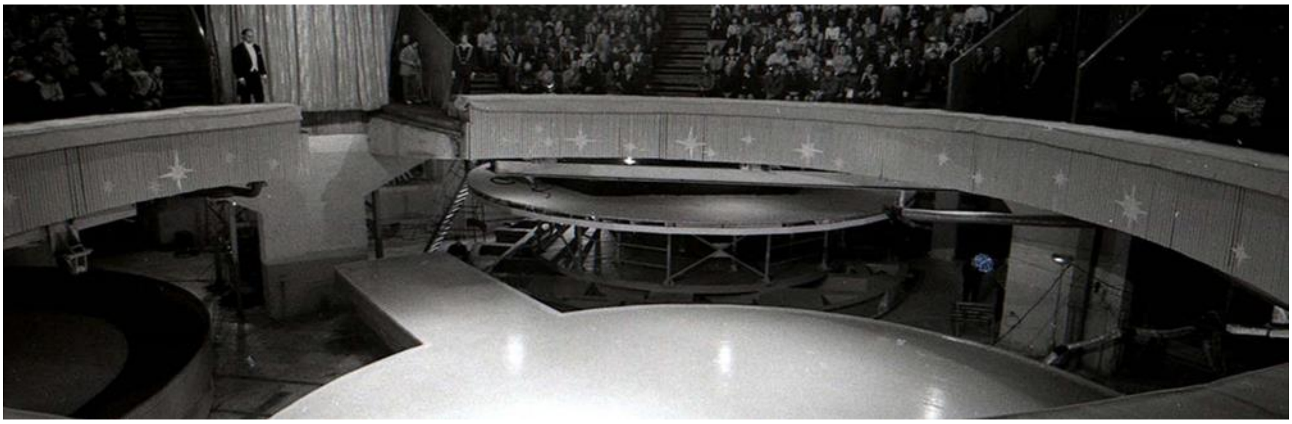

Figure 6: Platform change, 1972-1975, from the family archive of Dimitrij Vozdviženski (junior)

The most complex in its construction is the water platform. It is, in fact, a pool with windows, lighting and fountains. It is always raised empty and only when the installation is completed, the filling of 350 tons of water from a special tank begins. After the act is finished, all that water flows through the complex filter system back into the same tank, and only when all the water is collected can it be replaced with another platform. Maintenance of the water arena is the most expensive and takes the most time: it is necessary to regularly maintain and renew the filtration system, electronics, pipelines, and the water stage itself, ie the pool. The light podium consists of a transparent plastic circle on a pedestal with lighting, which is mounted on a fixed part of the stage.

The stage for performances with horses is a standard type of stage, which does not require special maintenance. The only thing you need to take care of is that the surface layer is in order, since it is expensive Vietnamese rubber. This coating must be completely flat so that people and animals are not injured. Freezing water on the ice platform is based on the principle of an ordinary refrigerator: at the bottom there is a system of tubes with coolant, which cools and freezes ordinary water. When the performance on ice is over, the playground returns to its place, and its surface is polished with certain machines. The play "Around the World in 130 Minutes" uses ice, water and a platform for horses. The final act in this play is considered the culmination of which the engineers are responsible: a twenty-meter fountain with a special design of light and sound. This state-of-the-art stage technology is less and less used in circus performances, in order to avoid possible damage. Like the whole circus, these machines and their systems require reconstruction, which is planned in the near future. The problem is that those factories that made parts, also for this mechanism, closed a long time ago, but specific modern workshops could certainly embark on this endeavor. [18]

Figure 7: Water podium

5. CONCLUSION

Considering the complex structure, specifics of architecture and applied technology, the Moscow circus, we revealed the spatial framework (at least one small part) needed for this type of artistic event. Going through the contents of this facility, many more questions and dilemmas arise - from the attitude towards animals, safety measures, self-sustainability of the facility, which require extensive research.

The circus spectacle was most interesting when it first appeared, in the 18th and 19th centuries. As a novelty and something never seen before, the plays attracted more attention than today. In modern times, we are surrounded by a large number of different cultural and entertainment forms of programs, and therefore the popularity of all these events is present in all fields.

Visiting circus troupes on Belgrade stages shows us that less demanding (in terms of stage equipment) circus-theater pieces can take place in more modestly equipped spaces, and even street ones (when the street scene becomes scenic). New circuses have stopped being built, but the question is whether the circus could have achieved such popularity if the performances had not taken place in specially built facilities.

REFERENCES

[1] „Circus and Performance Spaces", Proceedings of International Conference „UpSideDown - Circus and Space", Münster (Germany), 28 - 30 June, (2017), https://www.unimuenster.de/Kulturpoetik/en/zirkuswissenschaft/konferenz/UpSideDown2017.html

[2] A.J. Shner and R.E. Slavsky, „Circus Art" in Little Encyclopedia, Soviet Encyclopedia, Moscow (Russia), pp. 15-18, (1973)

[3] D. Jando, „Histoire mondiale du cirque", Jean-Pieere Delarge, Paris (France), p.82, (1977)

[4] E. Domingues Michelatto, A. Aguiar and A. de Pádua Carrieri, „Brasilian canvas circuses. A field in constant motion and symbolic transformation", Brazilian Journal of Management / Revista de Administração da UFSM., 2019, Vol. 12, Issue 2, pp.233-254, https://doi.org/10.5902/19834659, (2019)

[5] F. G. Bardian, „Soviet circus on five continents", Iskusstvo, Moscow (Russia), pp. 70-73, (1977)

[6] T. Markschiess-Van and J.N. Bernhard. „Artisten und zirkus plakate", Edition Leipzig, Leipzig (Germany), pp. 42, (1976)

[7] S.G. Zmuel and B.A. Mihanko, „Architectural typology of buildings and structures: Textbook for universities", Architectura-S, Moscow (Russia), pp. 151-154, (2004)

[8] M.Cairoli, „The architectural acoustic design for a circus: The case study of Rigas Cirks", Applied Acoustics, February 2021, p.173, https://doi.org/10.1016/j.apacoust.2020.107726, (2021)

[9] https://synthart.livejournal.com/188077.html

[10] G.Arrighi, „Synthesising circus aesthetics and science: Australian circus and variety theatre at the turn of the twentieth century", Early Popular Visual Culture, July 2018, 16(3), pp. 235-253, https://doi.org/10.1080/17460654.2019.1569843, (2018)

[11] http://niv.ru/doc/dictionary/brockhaus- efron/articles/214/cirk.htm

[12] S. Quintana, M. Fernandez and M. Machimbarrena, "The Circus-Theater of Albacete: Acoustic characterization and analysis of its double stage configuration", Applied Acoustics, February 2022, p.189, https://doi.org/10.1016/j.apacoust.2021.108574, (2022)

[13] O. Đurić, „Adria ide dalje: od Artističkog preduzeća do akcionarskog društva: 1948-1998.", Čigoja, Belgrade (Serbia), pp. 14, (1999)

[14] http://architektonika.ru/2007/06/27/zdanie_cirka_na_vernadskom_prospekte_v_moskve_1971_god.html

[15] M.Yu. Sorvina, „Circus in Russian films (1910-1989): the influence of the expressive means of the circus on the cinema", PhD Thesis, State Institute of Art Studies of Moscow (Russia), (2010)

[16] D.Efremov, „The Circus Buildings of the Former USSR: An Exceptional Landmark of International Modernism", Historic Environment: Policy & Practice; Jun-Sep 2020, Vol. 11 Issue 2/3, pp. 410-412, https://doi.org/10.1080/17567505.2020.1760007, (2020)

[17] https://zateevo.ru/?section=page&alias=cirk_manezhi

[18] http://xn--tvkultua-cch.xn--u-4tb/a%D1%80ticle/show/a%D1%80ticle_id/146284/

Engineering TODAY

VOL. 1 / NO. 1 / 2022

CONTENTS